Title
The Influence of Functionals on Density Functional Theory Calculations of the Properties of Reducible Transition Metal Oxide Catalysts

Journal
The Journal of Physical Chemistry C, 117(48)

ISSN
1932-7447

Authors
Getsoian, Andrew Bean
Bell, Alexis T

Publication Date
2013-12-05

DOI
10.1021/jp409479h

Peer reviewed

THE JOURNAL OF PHYSICAL CHEMISTRY C

Article

pubs.acs.org/JPCC

The Influence of Functionals on Density Functional Theory Calculations of the Properties of Reducible Transition Metal Oxide Catalysts

Andrew "Bean" Getsoian and Alexis T. Bell*

Department of Chemical and Biomolecular Engineering, University of California Berkeley, Berkeley, California 94720, United States

Supporting Information

ABSTRACT: Reducible transition metal oxides (RTMOs) comprise an important class of catalytic materials that are used for the selective oxidation and electro- and photochemical splitting of water, and as supports for metal nanoparticles. It is, therefore, highly desirable to model the properties of these materials accurately using density functional theory (DFT) in order to understand how oxide structure and performance are related and to guide the search for materials exhibiting superior performance. Unfortunately, accurate description of the structural and electronic properties of RTMOs using DFT has proven particularly challenging. The M06-L density functional, which has been shown to be broadly accurate for calculations of gas phase clusters, has recently become available to researchers carrying out calculations in the solid state, but its performance in determining the properties RTMOs has been little investigated. The aim of this work was to assess the performance of the M06-L functional for describing the structural and electronic properties of a family of RTMOs: MoO_2, MoO_3, and $Bi_2Mo_3O_{12}$. Lattice constants, band gaps, and densities of states calculated using the M06-L functional are compared to those obtained from DFT+U. We have also used the M06-L functional to determine the reaction barrier for propene activation over $Bi_2Mo_3O_{12}$, the rate-limiting step in the oxidation of propene to acrolein. We find that while DFT calculations carried out with the M06-L functional are roughly five times more expensive computationally than those performed with DFT+U, the results obtained using the M06-L functional provide sensible results for all properties investigated, while avoiding the necessary trade-off between accurate electronic structure and accurate thermochemistry that occurs in DFT+U.

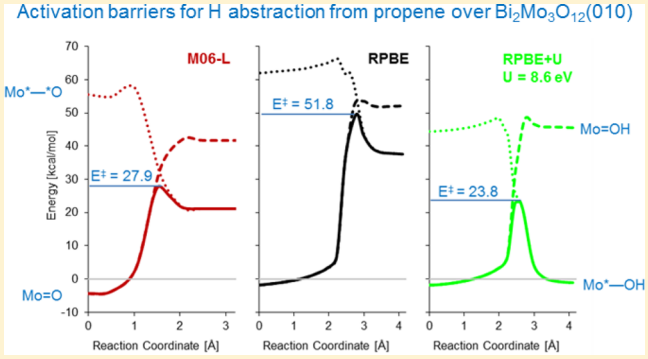

1.0. INTRODUCTION

Reducible transition metal oxides are used extensively as catalysts for the selective oxidation of hydrocarbons[1] and alcohols,[2,3] the reduction of nitric oxide,[4,5] the oxidation of sulfur dioxide,[6] the photochemical and electrochemical splitting of water to produce hydrogen and oxygen,[7,8] and the metathesis of olefins.[9,10] Each of these processes depends on the ability of transition metal centers in RTMOs to change oxidation states and to break or form bonds with reactant molecules. RTMOs also play an important role as supports for catalytically active metal nanoparticles, and in many cases such supports also serve as a promoter or as a cocatalyst. For example, the high CO oxidation activity of 2−3 nm gold particles supported on TiO_2 and CeO_2 has been found to depend, in part, on the formation of oxygen vacancies on the TiO_2 or CeO_2 support.[11−13] Electron transfer from oxygen vacancies in the support layer to the metal particle produces anionic gold, which efficiently activates dioxygen.[14,15]

Given the importance of RTMOs in catalysis, it is highly desirable to analyze the energetics of reaction pathways occurring on the surface of such materials with the aim of identifying the elementary processes governing reaction rates and product selectivities. To date, the most promising theoretical approach for analyzing the energetic of catalyzed processes has been density functional theory (DFT).[16−18] Extensive application of DFT has shown that when properly applied this approach can give highly accurate heats of adsorption and activation barriers in many instances for reactions carried out on metal nanoparticles, isolated metal oxo units, and active centers (e.g., Bronsted-acid protons and metal cations) contained in zeolites.[19] However, the application of DFT to the analysis of reactions occurring on RTMOs has proven to be particularly challenging. The primary difficulty arises from the tendency of DFT to exaggerate the extent to which electrons are delocalized.[20] This tendency arises from the erroneous self-interaction of electrons, a known inaccuracy in DFT resulting from the approximations used in constructing density functionals. Electron self-interaction error (SIE) is most problematic for open-shell systems of which RTMOs with partially occupied d subshells comprise an important subset.

Received: September 23, 2013
Revised: November 14, 2013
Published: November 15, 2013

Overdelocalization of electrons due to the SIE does not affect all RTMOs equally. For those systems in which d electrons are in fact delocalized, such as in RuO_2, accurate results from DFT have been attained.[21−23] However, DFT also predicts delocalization of electrons in many systems in which electrons are experimentally known to be well localized. A prime example of this phenomenon is seen for O vacancy formation in TiO_2. While wave function-based methods predict and experiments confirm that removal of an O atom from TiO_2 generates two localized Ti^{3+} states adjacent to the vacancy, standard DFT calculations distribute the two excess electrons over the entire TiO_2 crystal. As a result, DFT gives both inaccurate O vacancy formation energies and inaccurate geometries at O vacancy sites.[24] Vacancy formation in other systems suffers the same pathology,[25] a subject recently reviewed by Ganduglia-Pirovano et al.[26]

Inaccuracies due to electron SIE are not restricted to calculations of vacancy formation. A well-recognized failure of DFT arises in calculating the electronic structure of the simple oxide NiO. This compound is known experimentally to be a semiconductor with a band gap of 4.0−4.3 eV; however, NiO is predicted by many density functionals to have a band gap of only 0.4−0.6 eV,[27] or even no band gap at all.[28] Again, overdelocalization of the open-shell d electrons on the Ni atoms due to electron SIE is responsible for the incorrect prediction of the electronic structure in this and related materials. Even in less pathological cases than NiO, DFT is still generally found to underestimate band gaps as a consequence of the SIE.[29] The SIE also leads to poor descriptions of transition states,[30] and the absorption energies and structures of adsorbates bound to surfaces.[31,32]

The same SIE for unpaired electrons that leads to poor descriptions of energies and electronic structures in RTMOs also leads to inaccurate results for a far simpler system, the O_2 molecule. Popular density functionals like PBE, RPBE, and PW91 exhibit errors of 32, 26, and 21%, respectively, for the formation energy of O_2 from atomic O. Though less severely, these functionals also yield errors for the length of the O−O bond, of 3.0, 1.9, and 0.8% respectively. Erroneous prediction of the properties of O_2 further complicates calculations on the surfaces of RTMOs involving the adsorption, reaction, or evolution of O_2 molecules, processes which are involved in both oxidation chemistry and water electrolysis. While workarounds exist for the O_2 molecule specifically,[33] similar problems exist for related molecules including NO and superoxide anions. Again, electron SIE in systems with unpaired electrons is at the heart of the problem.

Several methods have been proposed to mitigate or eliminate the overdelocalization of electrons due to the SIE. Two of the most popular approaches are the DFT+U method and the hybrid DFT approach. In DFT+U, an extra interelectron repulsion term (U_{eff}) is introduced, the effect of which is to drive electron relocalization and thereby mitigate the effects of the SIE. Methods for determining the value of the interelectron repulsion from first principles have been proposed,[34−37] but in practice most researchers choose the value of this term in order to achieve agreement between a theoretically calculated and an observed property of a material of interest.[38−40] The DFT+U method has been applied successfully to the analysis of elementary processes on many RTMOs, including oxygen vacancy formation energies in TiO_2,[41] V_2O_5,[37] MoO_3,[42] and CeO_2;[43,44] activation of propene by $Bi_2Mo_3O_{12}$;[45] oxidation of methanol catalyzed by TiO_2-supported VO_x;[46] band bending and charge redistribution for TiO_2-supported Au;[47] and adsorbate binding in iron heme complexes.[48]

However, as presently used the DFT+U method suffers from two limitations. The first is that values of U_{eff} determined from self-consistent calculations are often at variance with the values found empirically to provide the best agreement between theory and experiment.[40] This limits the applicability of DFT +U to systems in which experimental data are already available. Second, the value of U_{eff} that provides the best agreement with experimental results typically depends on the experimental property of interest. A value of U_{eff} that provides an accurate description of the electronic structure of an oxygen vacancy in an RTMO may differ from the value that provides an accurate description of the vacancy formation energy. Even more problematic are cases where the optimal value of U_{eff} differs for the same element in different oxidation states or coordination environments.[35] In such a scenario, it is not clear how to conduct an accurate calculation on a reaction mechanism that involves a change in the oxidation state or coordination environment of the active site, and such changes are ubiquitous in the catalytic processes occurring on the surfaces of RTMOs.

An alternative approach for overcoming the effects of the electron SIE is to use hybrid density functionals, which complement the electron exchange of standard DFT with a fraction of Hartree−Fock-type exchange. Incorporation of Hartree−Fock exchange into DFT was first proposed by Becke,[49] and produces far superior results to those of DFT (or of pure Hartree−Fock theory) for a wide variety of material properties, including bond lengths, bond dissociation energies, reaction barriers, and frontier orbital energies. Hybrid functionals are now used extensively in theoretical studies of molecular chemistry and are being used increasingly in studies of the properties of solid-state material properties to determine band gaps[50,51] and oxygen vacancy formation energies.[26] The results of calculations carried out with hybrid functionals are also often used to determine a value of U_{eff} for subsequent DFT +U calculations.[42,52] However, due to the long-range nature of the Hartree−Fock exchange interaction, incorporating Hartree−Fock-like exchange into solid-state calculations involving periodic boundary conditions comes at a steep computational cost. Some progress toward limiting this cost has been made,[53] but the use of hybrid functionals remains a luxury for routine application to problems in solid-state chemistry. There are also certain classes of systems (including simple metals) where addition of Hartree−Fock-like exchange actually decreases the accuracy of the calculation.[54] Ultimately, the fraction of exact exchange used in a hybrid calculation is much like the value of U_{eff} used in a DFT+U calculation: the proportion of exact exchange yielding best agreement with experiment is dependent on the physical property of interest.

An ideal density functional approach for calculations on RTMOs should provide (1) accurate bond lengths and angles as well as accurate crystal lattice constants; (2) accurate descriptions of the electronic structure of RTMOs, including a correct description of the extent of localization of open shell electrons; (3) accurate bond formation and bond dissociation energies; (4) accurate adsorption energies, including physisorption and van der Waals interactions; (5) should contain no user-adjustable parameters; and (6) should be relatively inexpensive computationally. While it is not clear that an ideal density functional has yet been developed, the development of new density functionals is an active field of research.[55−57]

dx.doi.org/10.1021/jp409479h | J. Phys. Chem. C 2013, 117, 25562−25578

A functional that shows particular promise toward meeting the criteria listed above is the M06-L functional of Zhao and Truhlar.[58] This functional has been well benchmarked in molecular chemistry[59−61] and has seen application to a variety of systems involving reducible transition metals in molecular complexes[62−65] and cluster representations of extended solid surfaces.[66] The M06-L functional has recently been incorporated into the popular solid-state chemistry code VASP and has been shown to provide good performance in the calculation of band gaps for semiconductors[67] and the heat of adsorption of CO adsorption on metals.[68] The M06-L functional has also been implemented in the GPAW code,[69,70] and a few reports of the application of M06-L to solid-state calculations using this code have also been published.[71,72] Given the need for reliable density functional methods for performing calculations on RTMOs, and the initial success of M06-L in related systems, it is timely to investigate the performance of M06-L for calculations on RTMOs.

The purpose of this study is to investigate the performance of the M06-L functional for calculations on RTMOs, in order to determine how well it meets the "ideal functional" criteria listed above. Results obtained using the M06L functional are compared with those obtained from DFT+U and with experimentally measured properties. Three prototypical RTMOs were examined. The first is MoO_2, a metallic oxide which contains both one strongly localized and one strongly delocalized d electron per molybdenum atom. It therefore provides an interesting test for criterion (2). MoO_2 is also a catalyst for the isomerization of alkanes[73] and plays an active role in promoting the activity of MoO_2-supported Cu for the water gas shift reaction.[74] The second material is MoO_3, a medium band gap semiconductor with a layered structure; van der Waals forces play an important role determining its crystal structure. Standard density functionals have been shown to perform poorly in describing its crystal structure,[40] so MoO_3 provides a useful test for criteria (1) and (4). MoO_3 is catalytically active for the oxidative dehydrogenation of alkanes[75,76] including methane.[77] The energy for the reaction $H_2 + MoO_3 \Leftrightarrow MoO_2 + H_2O$ was used to choose the value of U_{eff} in previous DFT+U calculations on molybdates;[45] the energy for this process calculated by M06-L provides one test of criterion (3). Finally, for a comprehensive test of all of the criteria listed above, the activation barrier for the rate-determining step in the oxidation of propene to acrolein over $Bi_2Mo_3O_{12}$ was examined and compared to results from earlier work using DFT+U.[45] Propene oxidation over $Bi_2Mo_3O_{12}$ is a well-studied model for the selective oxidation and ammoxidation of light olefins over multicomponent bismuth molybdate-based catalysts, a process conducted industrially at the scale of 5 million ton per year.[78]

This paper is organized as follows. Section 2 provides a brief introduction to the DFT+U approach employed here. This section also provides some useful background on the M06-L functional and how its performance is expected to compare with that of DFT+U or of hybrid methods such as HSE. The computational methods employed are given in Section 3. The results given in Section 4 are broken into four parts. Section 4.1 compares the time required to perform a simple calculation using DFT, DFT+U, M06-L, and HSE, as per criterion (6) above. Section 4.2 presents some basic thermochemical results addressing criterion (3). Section 4.3 compares the performance of RPBE+U and M06-L for lattice constants and electronic structures, addressing criteria (1), (2), and (4). A detailed comparison of the mechanism by which propene is activated during oxidation over $Bi_2Mo_3O_{12}$ is presented in Section 4.4. Finally, our conclusions are given in Section 5.

2.0. AN INTRODUCTION TO DFT+U AND M06-L

In the simplified, rotationally invariant formulation of DFT+U applied here,[27] the self-consistent density functional energy is modified by imposing a penalty function

$$E_{\mathrm{DFT+U}} = E_{\mathrm{DFT}} + (U - J)\frac{1}{2}\sum_{lms}(n_{lms} - n_{lms}^2)$$

In principle, U is the coulomb potential, J is the exact exchange potential, and n is the occupation value of an atomic orbital with quantum numbers l, m, and s. (Because the plane wave basis sets used by VASP are not atom-centered, such atomic orbitals must be generated at the outset of the DFT+U calculation. This is done by projecting the plane waves onto spherical harmonic basis functions centered on selected atomic nuclei.) The difference $U - J$ is exactly the degree of uncanceled electron self-interaction and acts as a weight for a penalty function $n - n^2$ that drives the occupation value of n to either 1 or 0: each electron either entirely occupies or is entirely removed from a localized atomic orbital. While methods for determining U and J from first principles have been suggested in the literature,[34−37] in practice most researchers choose the value of the difference $U_{eff} = U - J$ empirically to match a known experimental constraint on the system of interest. Although in principle, a different value of U_{eff} could be applied to each orbital on each atomic center, ordinarily the correction is applied only to the d orbitals on transition metals, or the f orbitals on lanthanides and actinides (however, see refs 79 and 80 for an example in which a U_{eff} correction was applied to O 2p orbitals). In the present study, a U_{eff} term was applied only to the 4d orbitals on molybdenum.

In order to systematically examine the effect of the value of U_{eff} on lattice parameters, electronic structures, and reaction barriers, a range of U_{eff} values was investigated. We have used a U_{eff} value of 8.6 eV for Mo in previous RPBE+U calculations.[45] This value was chosen on thermochemical grounds: at U_{eff} = 8.6 eV, the RPBE+U method gives −84 kJ/mol for the energy change in the reaction $MoO_3 + H_2 \Leftrightarrow MoO_2 + H_2O$, in agreement with experiment (see refs 36 and 42 for more details). Coquet and Willock[42] have used a value of U_{eff} = 6.3 eV to calculate vacancy formation energies on MoO_3(010) by matching the spin density on reduced Mo centers in PBE+U calculations to the value obtained from a PBE0 reference calculation. The same value of U_{eff} has been adopted by Lei and Chen[81] in a subsequent investigation of H_2 adsorption on MoO_3(010). Values of U_{eff} = 2 and 4 eV have also been tested to provide a more complete examination of the U_{eff} parameter space for Mo.

The RPBE density functional to which DFT+U corrections have been applied belongs to a class of functionals known as GGAs, where GGA stands for generalized gradient approximation. The name signifies that these functionals use the value of the local electron density and its derivative in determining the energy of the system. Such functionals occupy the second rung of Perdew's "Jacob's Ladder" of density functionals[82] and have been widely used in chemistry and physics for at least 25 years. The M06-L functional takes a further step up this ladder and includes not only density and its first derivative, but also kinetic energy density (which is mathematically related to the

dx.doi.org/10.1021/jp409479h | J. Phys. Chem. C 2013, 117, 25562−25578

second derivative of density). Such functionals are called "meta-GGA". As Becke has nicely shown,[83] a significant amount of chemical information is embedded in the kinetic energy density, that is, the shapes of σ, π, and lone pair orbitals can be visualized directly from kinetic energy density maps. Becke[84] has also observed that information about the degree of electron delocalization can be extracted from a comparison between the kinetic energy density calculated from the Kohn−Sham orbitals and that calculated for a homogeneous electron gas (HEG) with the same local density: where electrons are strongly localized, these two densities are similar, whereas the HEG kinetic energy density becomes much smaller than the Kohn−Sham kinetic energy density in regions of electron delocalization. By calculating and comparing both types of kinetic energy density, a properly constructed meta-GGA functional can detect and correct for electron overdelocalization without including nonlocal HF-like exchange. Indeed, the M06-L functional contains a kinetic energy density-based term in its correlation functional that exactly removes the self-interaction error for a one-electron system.[85] In addition, the M06-L functional is semiempirical in that the values of 35 adjustable parameters used in its construction were optimized by "training" the functional on the collection of "test set" calculations. For systems whose chemistry is well represented in these test sets, the M06-L functional should therefore provide superior accuracy over PBE and RPBE, which contain no such empirical parameters. Notably, one of these test sets measures the ability of a density functional to capture noncovalent interactions, which are known to be poorly described in PBE and RPBE. The inclusion of noncovalent interactions in the training set for M06-L should improve its accuracy for describing systems in which noncovalent interactions are important.

The hybrid density functional scheme proposed by Heyd, Scuseria, and Ernzerhof[86,87] has also been investigated in the present work. Several researchers have shown that hybrid functionals provide superior accuracy to standard GGA methods in calculations on RTMOs.[26,49−51] The HSE functional[88] is constructed by (1) adding 25%[89] of Hartree−Fock-like[90] exchange to the PBE density functional (producing the hybrid commonly referred to as PBE0[91]), and (2) applying a range-screening correction to the Hartree−Fock-like exchange, such that the Hartree−Fock correction to the exchange interaction decays from 25% for short-range exchange coupling to 0% (i.e., pure PBE density functional exchange) for long-range exchange coupling. The range screening procedure allows the physically correct long-range cancelation between the PBE exchange and PBE correlation densities to be recovered and also reduces the computational expense of the functional compared to PBE0 in periodic systems.[92] Addition of short-range Hartree−Fock-like exchange significantly reduces the electron SIE in HSE calculations as compared to PBE, resulting in improved accuracy for atomization energies, geometries, and reaction barriers, while the use of pure PBE exchange in the long-range limit improves accuracy for metals and other naturally delocalized systems as compared to PBE0. Interestingly, HSE actually out-performs both its PBE and PBE0 parents for band gap calculations and geometries, though it is not as good as PBE0 for reaction barriers or atomization energies.[93] Since Hartree−Fock theory does not capture dispersive, noncovalent interactions, incorporation of screened Hartree−Fock-like exchange is not expected to improve the accuracy of the HSE hybrid functional for systems in which dispersive interactions are important.

3.0. THEORETICAL METHODS

All calculations were performed using VASP[94] version 5.3.2. DFT calculations were carried out using the PBE,[95] RPBE,[96] and M06-L[58,59] functionals. Hybrid DFT calculations were carried out using the HSE functional.[86,87] DFT+U calculations were carried out by applying the rotationally invariant, simplified formalism due to Dudarev et al.[27,97] Plane wave basis sets[98] were used to represent valence electrons, while core electrons were modeled using projector augmented waves[99,100] containing extra terms to allow calculation of the kinetic energy density contributions from core electrons.[101] The projector augmented wave cores used were designed for plane wave cutoff energies of 400 eV; this cutoff was used for calculations in the PBE, M06-L, and HSE functionals. Testing suggested that energy differences (e.g., between the MoO_2 and MoO_3 structures) were converged with respect to cutoff energy in the M06-L functional already at 400 eV. A larger cutoff energy of 500 eV was used for RPBE(+U) calculations for consistency with previous work.[45]

Convergence of the total energy with respect to k-point mesh was tested explicitly along each lattice axis. To determine the number of k-points required along the crystallographic a-axis, for example, a series of calculations were performed at $1 \times 1 \times 1$, $2 \times 1 \times 1$, $3 \times 1 \times 1$, $4 \times 1 \times 1$, and so forth k-points, and the total energy plotted as a function of the number of k-points used. The number of k-points was increased until an energy convergence of 0.5 meV/atom was achieved along each axis independently. For geometric relaxation (see next paragraph), an $8 \times 9 \times 8$ k-point grid was used for MoO_2, and a $6 \times 2 \times 6$ k-point grid was used for MoO_3. For $Bi_2Mo_3O_{12}$, a $4 \times 2 \times 3$ k-point grid was used for RPBE(+U) calculations, while a $3 \times 2 \times 2$ k-point grid was found to be sufficient when using M06-L. For density of states calculations, k-point grids were doubled: $16 \times 18 \times 16$ for MoO_2, $12 \times 4 \times 12$ for MoO_3, and $6 \times 2 \times 4$ for $Bi_2Mo_3O_{12}$. Timing comparison calculations on the RPBE, RPBE+U, M06-L, and HSE approaches were performed on MoO_2 using the same $6 \times 8 \times 6$ k-point mesh. Energies were converged using first-order Methfessel-Paxton energy smearing[102] for MoO_2 and Gaussian energy smearing for MoO_3 and $Bi_2Mo_3O_{12}$. A smearing value of 0.02 eV was used in all cases. For density of states calculations, energies were integrated over k-space using the tetrahedron method with Blöchl corrections.[103] No energy broadening was applied in density of states calculations.

To determine the optimal crystal structure in each functional, atomic positions in crystal structures taken from the literature[104−106] were allowed to relax at a series of fixed volumes. Total energy was plotted versus unit cell volume, and the third order Birch−Murnaghan equation of state[107,108] was used to fit the resulting curve. The minimum unit cell volume derived from this equation was selected, and the atomic positions in a cell of this volume allowed to relax until the total energy converged to within 0.1 meV.

To investigate propene activation over $Bi_2Mo_3O_{12}$, the $Bi_8Mo_{12}O_{48}$ unit cell was first cleaved along the crystallographic b-axis and a vacuum space of 12 Å introduced. The $Bi_8Mo_{12}O_{48}$ unit cell can be decomposed into four $Bi_2Mo_3O_{12}$ layers stacked along the b crystallographic axis. Of these, the top two layers were allowed to fully relax, while the bottom two layers were held fixed to their bulk positions. Propene was positioned over

dx.doi.org/10.1021/jp409479h | J. Phys. Chem. C 2013, 117, 25562−25578

the active site[45] on the relaxed surface, and the mechanism for hydrogen abstraction observed in previous work using RPBE +U was reinvestigated in the M06-L functional. The reaction path was determined by the nudged elastic band method[109] using the fast inertial relaxation engine algorithm developed by Bitzek et al.[110] and implemented in VASP by the Henkelman group.[111] The transition state for H abstraction from propene on $Bi_2Mo_3O_{12}$ occurs at the crossing between the singlet and triplet spin manifolds. To locate the transition state, spin-relaxed calculations were performed to generate the initial reaction path, with forces along the band converged to <0.1 eV/Å. The spin crossing point was then located using an algorithm described in detail elsewhere.[45]

Additional discussion is merited concerning use of the M06-L functional as implemented in VASP. The Minnesota family of functionals is known to require fine integration grids in order to provide accurate energies[112] (and in some cases, in order to converge at all). The default integration grid in VASP (as assigned through the variables NGX, NGY, and NGZ) was found to be too coarse for accurate evaluation of the M06-L functional, particularly for calculations involving slabs separated by vacuum space. Empirical testing suggested that an integration grid with 8 points per angstrom of lattice vector length was sufficient. Thus, for MoO_2 with lattice vectors 5.60 × 4.90 × 5.66 Å, an integration mesh of at least 44 × 40 × 44 should be used. Combined with an "accurate" precision setting, this leads to evaluation of the kinetic energy density on an 88 × 80 × 88 grid, which is sufficiently fine to provide converged results.

The most efficient algorithms for self-consistent convergence of the charge density and wave function in VASP (the Kosugi blocked-Davidson scheme and direct inversion of the iterative subspace) are not presently available for use with meta-GGA functionals. Use of the preconditioned conjugate gradient algorithm, the quick-min molecular dynamics algorithm, and the damped molecular dynamics algorithm was explored, and the conjugate gradient algorithm generally found to be most efficient. All methods worked well for calculations on bulk phases, while introduction of vacuum space into the calculation dramatically increased the number of self-consistent cycles required to reach convergence in each case. The slow convergence of the M06-L functional in systems containing significant vacuum space is a consequence of the way the exchange energy density functional in M06-L is constructed.[113] As the kinetic energy density goes to zero (as it does in the vacuum space far from the nuclei), the function that adjusts the exchange energy density in response to the kinetic energy density becomes ill-conditioned; small changes in the near-zero value of the kinetic energy density lead to large changes in the exchange energy density, which in turn lead to large changes in the total energy of the system.

Convergence of the M06-L functional is also sensitive to the initial guess provided. The default in VASP is to use a superposition of atomic densities for a guess at the charge density, and random numbers for the initial wave function. The use of random numbers leads to a very poor initial guess of the Kohn−Sham orbital kinetic energy density. As a result, the M06-L functional performs very poorly with the default initial guess, in many cases completely failing to converge. Therefore, an initial PBE or RPBE calculation was run prior to every M06-L calculation to generate better initial guesses for the charge density and wave function.

4.0. RESULTS AND DISCUSSION

4.1. Relative Computational Expense of RPBE, RPBE +U, M06-L, and HSE. Although listed last in the criteria for an optimal density functional in Section 1, reasonable computational expense is of primary importance for a density functional to be of practical use. Table 1 shows the relative lengths of time required to complete a calculation of the total system energy for MoO_2 at its experimental geometry with a 6 × 8 × 6 *k*-point mesh using the RPBE, RPBE+U (U = 8.6 eV), M06-L, and HSE functionals. Immediately obvious from Table 1 is the very high cost of the HSE functional relative to RPBE(+U) and M06-L. This high cost severely limits its utility for calculations on large, extended systems such as catalyst surfaces. Therefore, further calculations employing the HSE functional were not attempted in the present study. The HSE functional has been well benchmarked elsewhere.[86,114−117]

Table 1. Relative Computational Cost of Calculations on MoO_2

functional	relative time	SCF cycles
RPBE	1.0	14
RPBE+U (8.6 eV)	2.7	24
M06-L	9.7	14
HSE	3248	31

Although far less expensive than HSE, the M06-L functional is roughly an order of magnitude more expensive than the RPBE functional. (Note that part of the greater cost of this functional can be attributed to the finer integration grid required for its accurate evaluation, as discussed in Section 3.) Not included in the timing shown for the M06-L calculation is the time required to run an initial PBE (or RPBE) calculation in order to obtain a good initial guess for the charge density and wave function prior to carrying out an M06-L calculation. Attempting to converge an M06-L calculation without first reading in an initial guess for the charge density and wave function typically doubles the computational cost from that shown in Table 1 with the added cost coming entirely from the greater number of self-consistent iterations required to achieve convergence. Our experience has further shown that in many cases the M06-L functional will not converge in any number of iterations when an initial guess of the wave function is not provided. Thus, conducting an initial GGA calculation before using the M06-L functional is both faster and more reliable than using M06-L alone. In the case considered here, the computational cost of using the M06-L functional is roughly 10 times larger than that for the use of the RPBE functional and a factor of 4 more expensive than using the RPBE+U method. While relative job timings will be different for each system, the numbers given in Table 1 provide a useful illustration of the orders of magnitude involved.

4.2. Thermodynamic Considerations. In comparing the results of calculated reaction energies between DFT+U and M06-L, it is necessary to distinguish between results that are affected by altering the value of U_{eff}, and those that are not. Results for the latter category are shown in Table 2 for four reactions relevant to the chemistry discussed in Section 4.4. The first entry in Table 2 confirms a well-known result, that the PBE and RPBE functionals provide very poor descriptions of the O−O bond strength in O_2. The M06-L functional improves on these results substantially. Although it does not achieve "chemical accuracy" (usually considered to mean agreement

dx.doi.org/10.1021/jp409479h | J. Phys. Chem. C 2013, 117, 25562−25578

Table 2. Comparison of Thermochemical Accuracy for Different Functionals (kcal/mol)

reaction	PBE	RPBE	M06-L	experiment
$2\ O \rightarrow O_2$	−156.9	−149.3	−127.1	−119.0
$C_3H_6 \rightarrow C_3H_5 + H$	87.1	87.1	90.7	88.8
$H_2 + 1/2\ O_2 \rightarrow H_2O$	−58.0	−57.8	−57.3	−57.8
$C_3H_6 + O_2 \rightarrow C_3H_4O + H_2O$	−73.5	−109.2	−71.1	−79.4
mean absolute error	11.43	15.45	4.70	

with experimental values to within 1 kcal/mol), it does reduce the error by a factor of 3 versus RPBE and a factor of 4 versus PBE. All four functionals give "chemically accurate" results for the homolytic dissociation of propene and for the formation of water. For oxidation of propene to acrolein by oxygen, a reaction catalyzed by $Bi_2Mo_3O_{12}$, and discussed in greater detail in Section 4.4, chemical accuracy is not achieved by any functional. The PBE and M06-L functionals provide similar performance, while the RPBE functional significantly overestimates the exothermicity of this reaction. From the results in Table 2, it is evident that the M06-L functional does not provide perfectly accurate thermochemical results. However, it has by far the lowest mean absolute error for the examples considered here. This observation is in line with a previous, much more extensive investigation[118] in which the mean absolute errors for the PBE, RPBE, and M06-L functionals were found to be 7.8, 6.5, and 4.0 kcal/mol, respectively. It is difficult to predict how accurate a density functional will be for any particular reaction, as good agreement with experiment may reflect a better description of the underlying physics, but may also reflect a fortuitous cancelation of errors. However, the improved average accuracy of the M06-L functional compared to the PBE and RPBE functionals over a set of reactions is expected; because the M06-L functional is highly parametrized, and the values used in its parametrization were fitted to experimental data, the M06-L functional has more "built-in chemical knowledge" than PBE or RPBE.

For reactions involving transition metals, the thermochemical results become dependent upon the value of U_{eff} applied. Several researchers have argued in favor of choosing a value of U_{eff} based on the oxidation energy of the system of interest.[38,39] We have followed this approach in our previous work,[45] wherein a value of U_{eff} = 8.6 eV was chosen for Mo based on the change in energy for the reaction $MoO_3 + H_2 \Leftrightarrow MoO_2 + H_2O$. The choice of this reaction reflects a desire to tune U_{eff} in order to accurately describe the thermodynamics of oxidation and reduction on molybdenum. In principle, choosing the reaction $MoO_2 + O_2 \Leftrightarrow MoO_3$ should provide the same result. However, as Table 2 shows, the large error associated with the formation energy of O_2 introduces an extra complication in using the latter reaction.

Figure 1 shows the effect of the choice of U_{eff} on the calculated reaction energies for the reaction $MoO_3 + H_2 \rightarrow MoO_2 + H_2O$ determined using the PBE and RPBE functionals. Also shown are the energies for this reaction determined using M06-L functional, along with the experimental value. It is notable that although the energies calculated using the PBE and RPBE functionals differ significantly, the effect of U_{eff} on calculations using these functionals is essentially identical. Because the functional forms of the PBE and RPBE density functionals are very similar (they differ only by a minor change in the exchange enhancement function), it is not surprising that the U_{eff} correction acts similarly on both functionals. Given the essentially identical effect of the U_{eff} correction on the PBE and RPBE functionals, only the RPBE+U functional was investigated in the present study. It can be readily anticipated that results from PBE+U would follow the same trends.

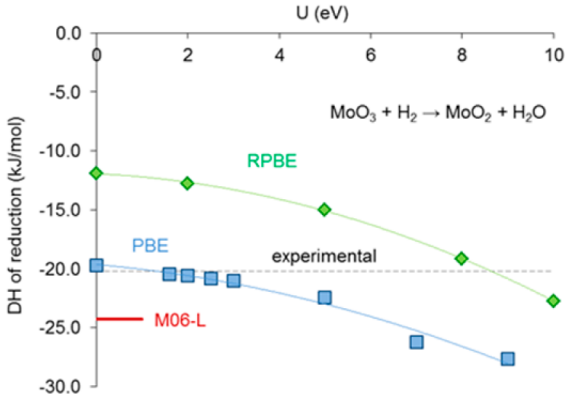

Figure 1. Reaction energy for the process $MoO_3 + H_2 \rightarrow MoO_2 + H_2O$ for different values of U_{eff} in the PBE (lower line, blue) and RPBE (upper line, green) density functionals. The experimental value of −20.2 kcal/mol is shown as a dotted line. The M06-L functional predicts a reaction energy of −24.3 kcal/mol (red mark).

4.3. Lattice Constants and Electronic Structures.

4.3.1. Molybdenum Dioxide (MoO_2). MoO_2 has a monoclinic crystal structure that can be derived from the tetragonal structure of rutile by pairing Mo centers along the rutile *c*-axis (which becomes the *a*-axis in the monoclinic cell definition) to produce covalent Mo−Mo bonds. The instability of a tetragonal (rutile) MoO_2 phase has been nicely demonstrated by Eyert et al.,[104] while the principles underlying the electronic structure of this phase were clearly elucidated by Goodenough[119] more than 40 years ago. In brief, metal centers in roughly octahedral coordination environments experience crystal field effects that split their d orbitals into e_g and t_{2g} sets. In rutile-based structures, the lower energy t_{2g} set is further split by the ability of d_{xy} orbitals on neighboring centers to overlap, forming σ-bonding pairs, while such overlaps are not possible for the d_{yz} and d_{xz} orbitals. Overlap between neighboring d_{xy} orbitals is strengthened if pairs of metal centers move toward each other along the rutile *c*-axis. The resulting distortion doubles the unit cell, and in the case of MoO_2, locks one d electron per Mo center into a covalent Mo−Mo bond. The other d electron from each Mo center occupies one of the degenerate d_{xz} and d_{yz} orbitals; half-filling of this degenerate band gives rise to the metallic conductivity of the oxide. The effective mass of the conduction electrons in MoO_2 is roughly three times that of a free electron, suggesting that unpaired d electrons in MoO_2 are not strongly correlated. Thus, the electronic structure of MoO_2 contains one strongly localized and one strongly delocalized d electron per Mo center. It should also be noted that MoO_2 is nonmagnetic at all temperatures.[104,120] Consistent with this observation, it was

dx.doi.org/10.1021/jp409479h | J. Phys. Chem. C 2013, 117, 25562−25578

Table 3. Lattice Constants for MoO_2 (Lengths in Angstrom; Volumes in Cubic Angstrom; U_{eff} Values in eV)

		RPBE					
	expt	U_{eff} = 0.0	U_{eff} = 2.0	U_{eff} = 4.0	U_{eff} = 6.3	U_{eff} = 8.6	M06-L
a	5.6109	5.6431	5.6421	5.6275	5.6383	5.6619	5.6025
b	4.8562	4.9523	4.9682	5.0000	5.0345	5.0618	4.8998
c	5.6285	5.7263	5.7434	5.7723	5.7900	5.8198	5.6596
β	120.95°	120.65°	120.65°	120.74°	120.67°	120.80°	121.52°
vol	131.53	137.67	138.50	139.60	141.36	143.27	132.43
				% Error			
a		0.57%	0.56%	0.30%	0.49%	0.91%	−0.15%
b		1.98%	2.31%	2.96%	3.67%	4.23%	0.90%
c		1.74%	2.04%	2.56%	2.87%	3.40%	0.55%
vol		4.67%	5.30%	6.14%	7.48%	8.93%	0.69%

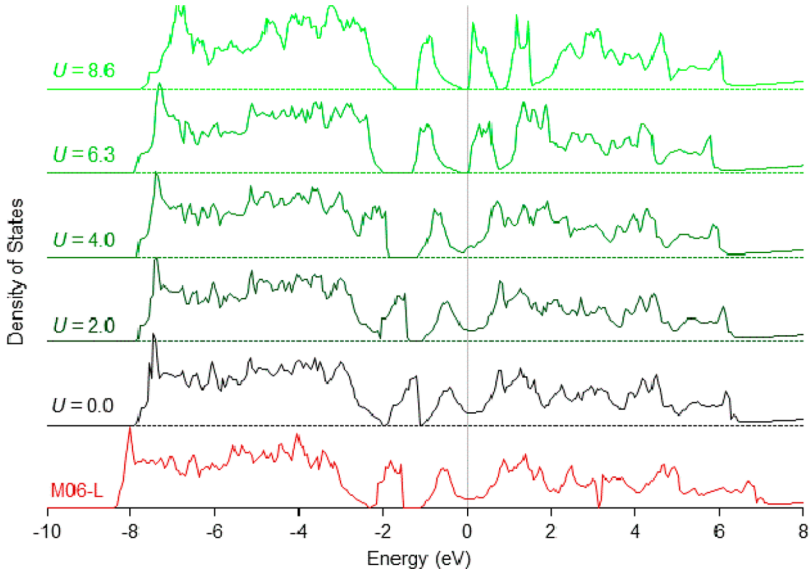

Figure 2. Density of states in MoO_2 in the M06-L and RPBE(+U) functionals. U_{eff} in eV. The Fermi level (0 eV) is set to the energy of the highest occupied state.

found that it was not necessary to perform spin-polarized calculations on this phase.

The effects of the choice of functional and value of U_{eff} on the lattice parameters of MoO_2 are shown in Table 3. The RPBE functional alone provides a reasonable match to the experimental lattice constants, but larger values of U_{eff} lead to increasing overestimation of the unit cell dimensions. On the other hand, the M06-L functional gives reasonably good values for lattice constants of MoO_2.

The valence band structure[121,122] of MoO_2 determined experimentally shows a primary O 2p bandwidth running from roughly −3 to −10 eV relative to the Fermi level. Two higher energy peaks also appear. Gulino et al.[120] place the first of these features at 1.4 eV below E_{fermi} and the second feature at 0.4 eV below E_{fermi}. Scanlon et al. find a similar result,[121] placing these peaks at 1.6 and 0.6 eV below E_{fermi}, respectively. The first peak is attributed to the Mo−Mo bond formed by σ-overlap of d_{xy} orbitals, as discussed above. The second peak is assigned to the singly occupied d_{xz}−d_{yz} state. On the basis of careful investigation of high-resolution ultraviolet photoelectron spectroscopy (UPS), Gulino et al. have concluded that this latter state should also have significant Mo−Mo π-bonding character. The lowest unoccupied states are expected to appear roughly 2.5 eV above the top of the O 2p valence states.

The effects of the choice of functional and the value of U_{eff} on the density of states in MoO_2 are shown in Figure 2. All calculations underestimate the width of the valence band, which terminates at −8 eV versus E_{fermi} for the RPBE(+U) calculations, and −8.5 eV for the M06-L calculations. The RPBE and M06-L calculations both capture the features of the experimentally observed MoO_2 valence band: the material is metallic with two distinct features sitting between the main valence band and the conduction states. RPBE places these features at −1.4 and −0.5 eV relative to the Fermi level, while M06-L places the Mo−Mo bond orbital at −1.9 eV and the d_{xz}−d_{yz} state at −0.6 eV. Switching on the Hubbard U term in the RPBE calculation preserves these features initially; the Mo−Mo bonding band shifts to slightly lower energy at U_{eff} = 2 eV but the material remains metallic. As U_{eff} increases to 4 eV, the Mo−Mo bonding band begins to merge with the main valence band. The occupied Mo d conduction states also shift to lower energy, and begin to decouple from the conduction band. When U_{eff} is increased to 6.3 eV, the Mo−Mo bonding band vanishes completely into the valence states, and the remaining occupied Mo d states shift below the Fermi level, opening up a very arrow (∼0.2 eV) band gap. The antibonding states in the conduction band above the Fermi level also begin to narrow and separate; of these, the one closest to the Fermi level is most well-resolved. When U_{eff} is further increased to 8.6 eV, the

dx.doi.org/10.1021/jp409479h | J. Phys. Chem. C 2013, 117, 25562−25578

Table 4. Lattice Constants for MoO_3 (Lengths in Angstrom; Volumes in Cubic Angstrom; U_{eff} Values in eV)

		RPBE						
	expt	PBE	U_{eff} = 0.0	U_{eff} = 2.0	U_{eff} = 4.0	U_{eff} = 6.3	U_{eff} = 8.6	M06-L
a	3.9628	3.9630	4.0883	4.0490	4.0275	3.9971	3.9665	3.9317
b	13.855	16.548	17.097	17.160	17.118	17.102	17.094	13.028
c	3.6964	3.7100	3.7014	3.7188	3.7373	3.7655	3.7973	3.7037
vol	202.95	243.29	258.71	258.39	257.66	257.41	257.47	189.72
				% Error				
a		0.01%	3.17%	2.18%	1.63%	0.87%	0.09%	−0.79%
b		19.43%	23.40%	23.85%	23.55%	23.44%	23.38%	−5.97%
c		0.37%	0.13%	0.61%	1.11%	1.87%	2.73%	0.20%
vol		19.88%	27.48%	27.32%	26.96%	26.83%	26.87%	−6.52%

states above the Fermi level continue to narrow and a 0.2 eV band gap continues to be present between the highest occupied and first unoccupied Mo d state. These results are consistent with the expectation that for a sufficiently large value of U_{eff}, any metal oxide with partially occupied d orbitals will become a Mott-Hubbard insulator. The results presented here suggest that in order to achieve a qualitatively correct description of the electronic structure of MoO_2, a value of U_{eff} < 4 eV should be employed with the RPBE functional.

4.3.2. Molybdenum Trioxide (MoO_3). MoO_3 is a medium band gap semiconductor. Although methods like PBE are known to underestimate the band gap, the problem is one of degree, not of kind: DFT does not erroneously predict metallic behavior for this material. MoO_3 does, however, present a different challenge for DFT in that its structure is comprised of layers with strong iono-covalent bonds holding the material together within each layer but only van der Waals forces binding these layers to each other. As seen in Table 4, simple density functionals such as PBE and RPBE are unable to capture these dispersive interactions adequately, leading to dramatic failures in the prediction of lattice constants. All lattice constants are overestimated to some degree, but the errors along the *b*-axis along which weakly bound layers are stacked exceed 20%. Functionals that perform so poorly for van der Waals interactions will also seriously underestimate the heats of adsorption of molecules on surfaces, and the nature and degree of surface reconstruction that surfaces experience upon being cleaved from the bulk. They are also likely to underestimate the strength of hydrogen bonds, which ultimately are more dispersive than covalent in nature. If the strength of hydrogen bonding interactions is underestimated, then for calculations on surfaces reacting in an aqueous environment (e.g., for a model of an electrochemical process), even calculations including explicit water layers above the surface may not properly capture the nature of the interactions taking place between surface, adsorbate, and solvent. Such interactions can be decisive in determining operative mechanisms under electrochemical conditions.[123]

Table 4 also shows that the value of U_{eff} has only a small effect on lattice constants in MoO_3. Increasing the value of U_{eff} lengthens the **c**-vector slightly at the expense of the **a**-vector, reflecting changes in the degree of hybridization between empty Mo d states and the empty Mo s and p states responsible for Mo−O bonding interactions. The *b*-lattice constant is almost totally unaffected by the value of U_{eff}. Since there are no occupied d orbitals on MoO_3 on which a Hubbard *U* correction could act directly, it is reasonable that the overall effects of U_{eff} on lattice constants in MoO_3 are small.

Compared to PBE and RPBE(+U), the M06-L functional yields a much more accurate estimate of the lattice constants for MoO_3. In fact, the M06-L functional actually underestimates the length of the **b**-vector. More detailed analysis reveals that M06-L accurately describes the axial Mo═O bonds (1.693 Å experimentally; 1.695 Å with M06-L), while overestimating the iono-covalent Mo−O bond along the *b*-axis within each layer (2.258 Å experimentally; 2.373 Å with M06-L). Planes of terminal oxygens in adjacent layers are too close together (0.478 Å experimentally; 0.313 Å with M06-L) but this only shortens the nearest interlayer O−O contact from 2.77 Å to 2.74 Å. It is also noted that the M06-L functional does not contain empirical dispersion, and hence, its successful description of van der Waals interactions is due entirely to the parametrization of its exchange-correlation functional. The relative success of the M06-L functional in describing the structure of MoO_3 is consistent with the observation that this functional provides improved descriptions of the structures of graphite, hexagonal boron nitride, and MoS_2, each of which possesses a two-dimensional layered structure.[124]

Band gaps calculated for MoO_3 using each functional are given in Table 5. Figure 3 shows the corresponding densities of states. To facilitate comparisons among band gaps and valence band widths, the Fermi level in Figure 3 has been set to the top of the valence band, rather than to the center of the band gap as would be conventional for a semiconductor. As expected, the PBE and RPBE functionals underestimate the band gap, the PBE functional in particular erring by ∼40%. Unexpectedly, small values of U_{eff} reduce the band gap to values even lower than those obtained for U_{eff} = 0 though the effect is small. Larger values of U_{eff} do have the expected effect of widening the band gap, but again the effect is small. Even at the largest value examined here, the band gap is still well short of the experimental value. Since there are no occupied d orbitals in this system for which the energies can be examined, and since even large values of U_{eff} do not reproduce the experimental

Table 5. Band Gaps for MoO_3

functional	band gap (eV)
PBE	1.79
RPBE	2.19
RPBE+U (2.0 eV)	2.09
RPBE+U (4.0 eV)	2.14
RPBE+U (6.3 eV)	2.19
RPBE+U (8.6 eV)	2.38
M06-L	2.15
experiment	2.98

dx.doi.org/10.1021/jp409479h | J. Phys. Chem. C 2013, 117, 25562−25578

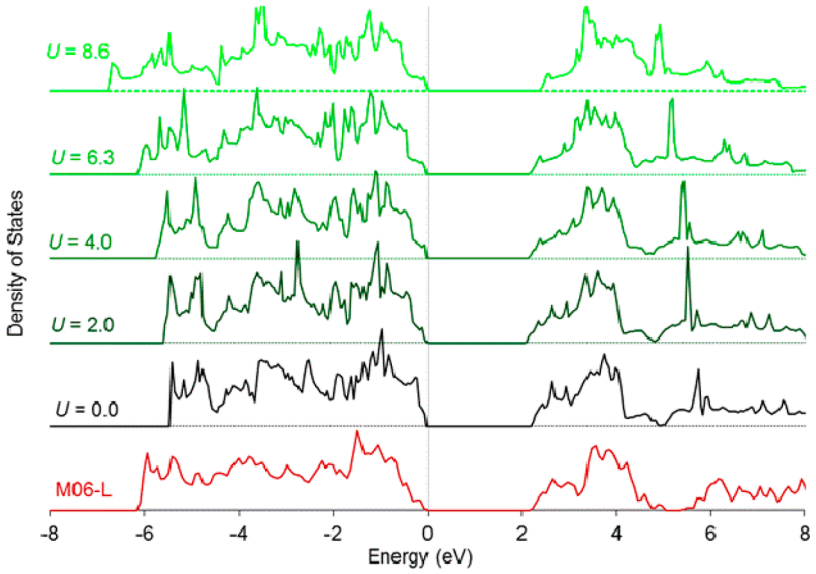

Figure 3. Density of states in MoO_3 in the M06-L and RPBE(+U) functionals. U_{eff} in eV. The Fermi level (0 eV) is set to the energy of the highest occupied state.

band gap, it is not obvious how to choose an appropriate value of U_{eff} on the basis of the densities of states in Figure 3. Indeed, the relative insensitivity of the results in Tables 3 and 4 and Figure 3 to the value of U_{eff} suggest that a +U correction is neither harmful nor helpful for achieving more accurate lattice constants or densities of states for MoO_3. However, the total energy of the system as calculated within VASP does vary with the value of U_{eff} (as seen in Figure 1). Larger values of U_{eff} also lead to stronger Mo−O bonds, visible in Figure 4 as a shift in

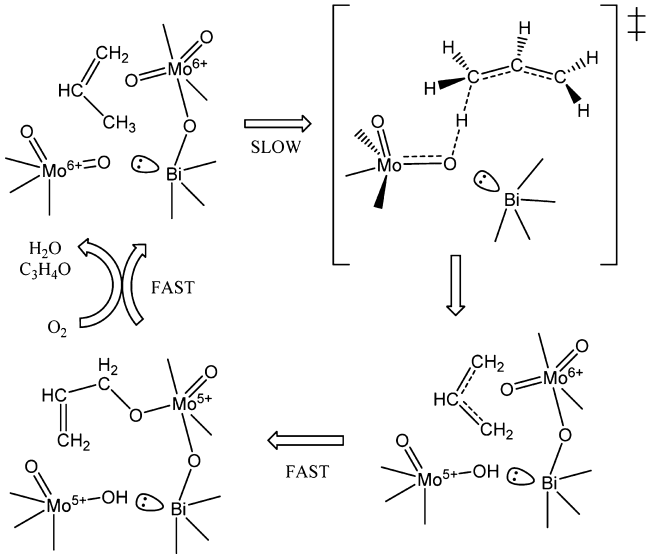

Figure 4. Mechanism for propene activation over $Bi_2Mo_3O_{12}$.

the bottom of the valence band to lower energies. The M06-L functional also underestimates the band gap as compared to experiment; its performance is on par with that of RPBE.

4.3.3. Bismuth Molybdate ($Bi_2Mo_3O_{12}$). The alpha phase of bismuth molybdate, $Bi_2Mo_3O_{12}$, is an active catalyst for the selective oxidation of hydrocarbons.[45,78,125,126] Its crystal structure can be derived from the scheelite ($CaWO_4$) structure by (1) creating an ordered array of cation vacancies at one-third of the Ca^{2+} sites, while placing Bi^{3+} ions at the other two-thirds of the Ca^{2+} sites; and (2) rotating pairs of tetrahedral MoO_4^{2-} ions toward each other to create $Mo_2O_8^{4-}$ dimers containing five-coordinate Mo^{6+} ions. The presence of many cation vacancies and Mo═O double bonds gives $Bi_2Mo_3O_{12}$ a layered structure with few covalent bonds connecting layers along the crystallographic *b*-axis. Thus, as in MoO_3, dispersive interactions play an important role in determining the overall lattice constants and atomic positions within the structure.

Table 6 compares the experimentally measured lattice constants of $Bi_2Mo_3O_{12}$ to those calculated using the RPBE

Table 6. Lattice Constants for $Bi_2Mo_3O_{12}$ (Lengths in Angstrom; Volumes in Cubic Angstrom; U_{eff} = 8.6 eV)

	expt	RPBE+U	M06-L
a	7.7104	8.0186	7.7426
b	11.5313	12.2491	11.7374
c	11.972	12.308	12.065
β	115.276°	114.029°	116.057°
vol	962.53	1103.75	984.99
% Error			
a		4.00%	0.42%
b		6.22%	1.79%
c		2.81%	0.78%
vol		11.47%	2.33%

functional with U_{eff} = 8.6 eV and those calculated using M06-L. As with MoO_3, the value of U_{eff} chosen had little effect on lattice constants for a material containing no occupied d orbitals (not shown). The tendency of the RPBE functional to overestimate lattice constants is evident from Table 6. As noted above, the particularly large error for the **b**-lattice vector is a result of the importance of dispersive forces along this axis. By contrast, the M06-L functional yields much better agreement with the experimentally determined lattice constants for $Bi_2Mo_3O_{12}$.

The band gaps calculated for $Bi_2Mo_3O_{12}$ using RPBE+U and M06-L are given in Table 7. As for MoO_3, the RPBE functional significantly underestimates the band gap. Here, however,

dx.doi.org/10.1021/jp409479h | J. Phys. Chem. C 2013, 117, 25562−25578

Table 7. Band Gaps for $Bi_2Mo_3O_{12}$

functional	band gap (eV)
RPBE	2.55
RPBE+U (2.0 eV)	2.60
RPBE+U (4.0 eV)	2.70
RPBE+U (6.3 eV)	2.85
RPBE+U (8.6 eV)	3.05
M06-L	2.72
experiment	2.95

increasing the value of U_{eff} does have a significant impact on the estimated band gap with the largest value tested, U_{eff} = 8.6 eV, actually leading to an overestimation with respect to experimental values. The experimental gap of 2.95 eV could be matched by using U_{eff} = 7.5 eV. The M06-L functional improves significantly on the RPBE functional but still falls short of the experimental value.

The densities of states for $Bi_2Mo_3O_{12}$ calculated using the RPBE+U and M06-L functionals are available in the Supporting Information. They differ from the spectra shown in Figure 5 (discussed below) only in that the states marked (★) and (■) do not appear in the spectra for $Bi_2Mo_3O_{12}$. To the best of our knowledge, an experimental investigation of the valence or conduction band states in $Bi_2Mo_3O_{12}$ has not been reported.

4.4. Propene Activation by Bismuth Molybdate. We have recently reported an analysis of the mechanism by which propene is oxidized to acrolein on the surface of $Bi_2Mo_3O_{12}$ carried out using DFT and the RPBE+U method.[45] The principle objectives of that work were to investigate the energetics of the mechanism deduced from experiments and to define the active site requirements for propene activation. As discussed in Section 2, a value of U_{eff} = 8.6 eV was used in order to obtain accurate thermochemical results for catalytic steps over $Bi_2Mo_3O_{12}$ that involved reduction at Mo centers.

As shown in Figure 3, the rate-determining step in the conversion of propene to acrolein is abstraction of a hydrogen atom from the methyl group of propene by a lattice oxygen atom. At the transition state, the double bond of an Mo═O group is broken, producing a reduced Mo^{5+} center and an electrophilic O^- center. The electrophilic O^- then abstracts H from propene, producing an allyl radical and converting the Mo^{6+}=O active site to Mo^{5+}−OH. The most active Mo^{6+}=O site was found to be one with a Bi neighbor 2.7−2.8 Å from O, and additional calculations suggested that further decreasing this Bi−O distance would decrease the propene activation barrier. The intrinsic activation barrier for propene activation determined using RPBE+U is 25.0 kcal/mol at the most active Mo═O site. When combined with an experimentally measured heat of adsorption of 7−8 kcal/mol,[127,128] this yields an apparent activation barrier of 17−18 kcal/mol, in excellent agreement with the experimentally measured range of 17−21 kcal/mol.[124,125]

While the activation barriers found in ref 45 are in good agreement with experimental values, the analysis in Section 4.3.1 demonstrates that for at least one phase containing reduced molybdenum centers, a U_{eff} value of 8.6 eV introduces significant distortions into the calculated electronic structure of the material. Since propene activation over $Bi_2Mo_3O_{12}$ leads to the creation of reduced molybdenum centers, it was of interest to determine the effect the value of U_{eff} on the density of states of reduced $Bi_2Mo_3O_{12}$. Figure 5 shows the majority spin density of states for the $Bi_2Mo_3O_{12}$ slab after activation of propene. On the catalyst surface, one Mo^{6+}═O active site has been converted to Mo^{5+}−OH, while the propene molecule has been converted to an allyl radical physisorbed nonspecifically over the slab. For clarity, the states attributable to the allyl radical in Figure 5 have been removed; the energies of those states are not affected by changes in the value of U_{eff}. The Fermi level in Figure 5 has been set to the energy of the highest doubly occupied state (i.e., excluding the unpaired electron on Mo^{5+}) to facilitate comparison among the spectra.

When U_{eff} = 0 eV, the occupied Mo *d* state (marked with a ★ in Figure 5) sits at the top of the band gap. As the value of U_{eff}

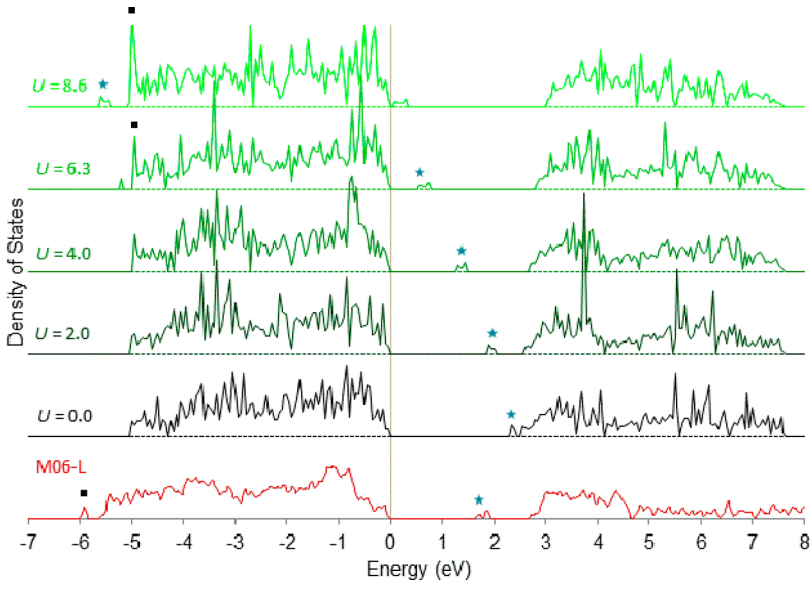

Figure 5. Majority spin density of states in $Bi_2Mo_3O_{12}$ with one surface Mo^{6+}═O group replaced by Mo^{5+}−OH. The Fermi level (0 eV) has been set to the energy of the highest occupied minority spin state, that is, to the highest occupied state excluding the unpaired d electron on Mo^{5+}. The state occupied by the unpaired d electron is marked with a blue star. The state marked with a black square in the M06-L, U = 6.3, and U = 8.6 spectra represents the O−H bond. For U = 0.0, U = 2.0, and U = 4.0, this state occurs in the O 2s region at −22 eV, and is therefore not visible in the figure.

dx.doi.org/10.1021/jp409479h | J. Phys. Chem. C 2013, 117, 25562−25578

is increased, the energy of this state decreases, such that it moves into the middle of the band gap for U_{eff} = 2−4 eV. The character of this state also changes with the value of U_{eff}: for U_{eff} = 0−2 eV, it has essentially pure Mo d character but by U_{eff} = 4 eV it begins to take on some O p character. This effect becomes pronounced as U_{eff} rises to 6.3 eV; the state has now decreased in energy to nearly the bottom of the band gap, and now has principally O p character. As U_{eff} rises further to 8.6 eV, the singly occupied state becomes purely O 2p in character. The occupied Mo 4d state has instead emerged below the valence band at an energy near −5.5 eV. A similar effect has been observed[40] in calculations on reduced V_2O_5 with U_{eff} = 6 eV. Also marked in Figure 5 for the M06-L, U = 6.3, and U = 8.6 eV spectra is a state having a mixture of O 2p and H 1s character. This state represents the O−H bond formed by attachment of H to the surface during the activation of propene (see Figure 4). When U_{eff} is 4 eV or less, no H 1s character can be detected in any state in the valence region. Instead, the H 1s state appears among the O 2s states near −22 eV (not shown in Figure 5). Thus, the value of U_{eff} affects not only the energy of the Mo 4d orbitals but also the energy and position of the O−H bond proximal to the reduced Mo atom. The spectrum for M06-L shown in Figure 5 also shows an O 2p−H 1s bonding state, near −6 eV. The occupied Mo 4d state appears in the band gap at ∼1.8 eV above the bottom of the valence band.

The results in Figure 5 show that in reduced $Bi_2Mo_3O_{12}$, as in MoO_2, the value of U_{eff} has a significant effect on the calculated electronic structure. In the case of MoO_2, it was possible to compare the calculated electronic structures to experimental results in order to determine which calculations were most accurate. Ideally, the same procedure would be followed for reduced $Bi_2Mo_3O_{12}$. However, to our knowledge the electronic structure of slightly reduced $Bi_2Mo_3O_{12}$ has not been measured. Experimental studies on the reduction of related materials, such those of Grzybowska et al.[129] for Bi_2MoO_6 and MoO_3, typically reveal the emergence of a pair of states at ∼1 and ∼2 eV above the valence states, and the presence of Mo^{4+}. Such studies suggest that the features seen in the electronic structure of MoO_2 are general to molybdates containing the Mo^{4+} oxidation state. If it can be assumed that the properties of Mo^{5+} sites are also similar across different molybdate phases, then the results of Irfan et al.[130] are informative. These researchers conducted ultraviolet photoelectron spectroscopy (UPS) on MoO_3 films prepared by a vapor phase deposition procedure known to create slightly oxygen deficient MoO_3. UPS analysis of these films revealed a single occupied state ∼2 eV above the oxygen valence edge, and no evidence for a state 1 eV above the valence edge. Kanai et al.[131] also observed the appearance of a single state ∼2 eV above the valence band in MoO_3 films partially reduced by an electron-donating organic molecule in a model organic electroluminescent device and confirmed by X-ray photoelectron spectroscopy that this state was due to the presence of Mo^{5+}. If the energy level of an occupied d orbital on an Mo^{5+} center in reduced $Bi_2Mo_3O_{12}$ is similar to that observed on Mo^{5+} centers in reduced MoO_3, then the spectra in Figure 5 produced using the M06-L functional and the RPBE functional with $U_{eff} \leq 2$ eV are likely to be most accurate, in agreement with the findings of Section 4.3.1 for MoO_2. In any case, the placement of the occupied Mo 4d state below the valence band when U_{eff} = 8.6 eV is almost certainly not correct; if Mo 4d states existed at energies below those of the O 2p states, then in materials like $Bi_2Mo_3O_{12}$, electrons would spontaneously shift from O 2p states to Mo 4d states, reducing the material and releasing O_2, an effect that is not observed experimentally. Thus, it can be concluded that while RPBE+U calculations with U_{eff} = 8.6 eV can accurately describe the energetics of propene activation over $Bi_2Mo_3O_{12}$, they cannot accurately describe the electronic state of the partially reduced catalyst produced by this reaction. As a result, processes like adsorption of O_2 over a reduced Mo site in the catalyst, a process not examined in ref 45 but likely involved in the reoxidation of the catalyst after propene oxidation, may not be accurately described by RPBE +U calculations.

In addition to altering the energy of the occupied Mo 4d state significantly, the value of U_{eff} used also has a dramatic effect on the calculated activation barrier for the rate limiting step in propene oxidations (see Figure 4). Table 8 shows that

Table 8. Effect of U_{eff} (in eV) in RPBE+U Calculations on the Activation Barrier and Final State Energies (in kcal/mol) for Hydrogen Abstraction from Propene over $Bi_2Mo_3O_{12}$

U_{eff}	barrier	final state
0.0	54.6	37.2
2.0	52.9	30.2
4.0	46.8	21.9
6.3	38.9	11.0
8.6	25.0	0.7

turning off the +U correction drives the reaction barrier for propene activation to >50 kcal/mol, far beyond the experimentally measured range. The energy of the final state after hydrogen abstraction (Mo^{5+}−OH + allyl radical) relative to the initial state (Mo^{6+}=O + physisorbed propene) is given as well in Table 8. This column underscores the dramatic impact of the value of U_{eff} on the overall energy of reaction: the final state structure is identical in each case, and the energy of the allyl radical is unaffected by the $+U$ correction on molybdenum. Thus, the difference in final state energies at different values of U_{eff} directly reflects the relative degree of stabilization of the occupied Mo d orbital. For small values of U_{eff}, the final state energies grow significantly larger than the experimentally measured activation barrier. Thus, a comparison of the initial and final state energies determined using the uncorrected RPBE functional could lead to the incorrect conclusion that $Bi_2Mo_3O_{12}$ is not a competent catalyst for performing the oxidation of propene, in contradiction to experimental evidence. On the other hand, for a U_{eff} as large as 8.6 eV, the abstraction of hydrogen from propene becomes a nearly thermoneutral process — a surprising result given that a free radical is generated by this reaction. What Table 8 makes clear is that applying a +U correction to RPBE calculations on $Bi_2Mo_3O_{12}$ allows one to obtain a reaction barrier consistent with experimental findings, but only by introducing one error to cancel another. Overstabilization of an occupied Mo d orbital energetically compensates for an otherwise under-predicted reduction energy (as seen in Figure 1), but at the cost of yielding an inaccurate description of the resulting electronic structure (as seen in Figure 5). In this system, no value of U_{eff} is capable of providing chemically sensible results for both the reaction thermochemistry and the electronic structure of the reduced catalyst.

Figure 6 compares the reaction paths for the first hydrogen abstraction step determined from calculations carried out using the RPBE, RPBE+U (8.6 eV), and M06-L functionals. The zero

dx.doi.org/10.1021/jp409479h | J. Phys. Chem. C 2013, 117, 25562−25578

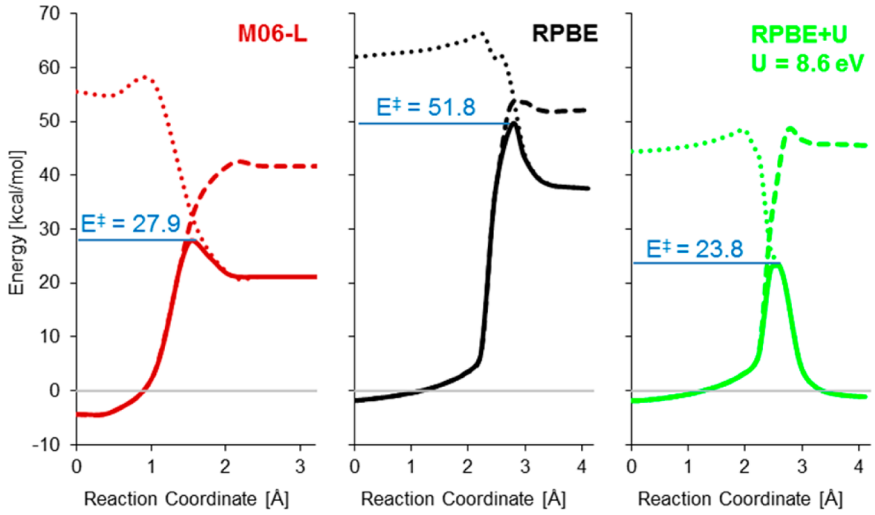

Figure 6. Activation barriers for hydrogen abstraction from propene over $Bi_2Mo_3O_{12}$ calculated using M06-L, RPBE, and RPBE+U (8.6 eV). The singlet spin states are indicated by long dashes, the triplet spin states by short dots, and the spin-coupled reaction paths by solid lines. The zero of energy (gray line) is set by the energy of the bare slab and gas phase propene taken separately.

in this figure is the sum of the energies of the bare catalyst surface and gas phase propene. The energy in each case starts below zero, reflecting physisorption of propene onto the catalyst surface. The M06-L physisorption energy is 4.4 kcal/mol, as compared to only 1.8 kcal/mol with RPBE(+U). This difference reflects the better ability of M06-L to capture the dispersive interactions responsible for physisorption. The experimental value for the heat of adsorption of propene is 7−8 kcal/mol.[127,128]

Following propene adsorption, the energy rises steeply and reaches a maximum at the transition state for hydrogen abstraction. This transition state occurs at the crossing between the spin-singlet and spin-triplet configurations of the system. In the transition state as calculated using RPBE+U with U_{eff} = 8.6 eV, the singlet−triplet transition arises from a rehybridization of a closed shell Mo(+6)═O(−2) bond to form an Mo(+5)*—*O(−1) diradical. This bond breaking step is the rate-determining event in the RPBE+U calculations, and occurs prior to the hydrogen abstraction step. As shown in Figure 7a (reproduced here from ref 45), the C−H bond has only barely stretched from its initial length of 1.10 Å, while the O−H distance of 1.58 Å indicates that formation of the O−H bond has only just begun. The Mo−O bond distance at the transition state, however, is 2.03 Å, significantly longer than the value of 1.76 Å prior to reaction and nearly equal to its final length of 2.05 Å. This distance is characteristic of a Mo−O single bond.

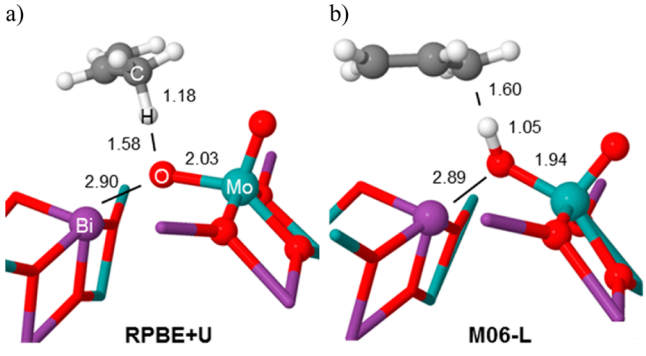

Figure 7. Transition states for hydrogen abstraction from propene calculated using RPBE+U (U_{eff} = 8.6 eV) (a) and M06-L (b). Distances are in angstroms. For clarity, atoms in the catalyst surface not directly involved in the chemistry are not pictured.

As shown in Figure 7b, when the calculation is conducted instead using the M06-L functional, a rather different picture of the transition state emerges. As in the cases where calculations were carried out using the RPBE+U functional, the M06-L functional predicts an Mo−O bond length of 1.94 Å in the transition state: stretched significantly from the initial value of 1.71 Å for the Mo═O double bond, and near to the value of a 2.00 Å Mo−O in the final state. Unlike the results obtained using RPBE+U, however, the C−H distance is stretched from 1.09 Å before reaction to 1.60 Å at the transition state, indicating that C−H bond dissociation is nearly complete when the transition state is reached. Conversely, the O−H distance is only 1.05 Å, close to its final value of 0.96 Å. Thus, the M06-L results predict that Mo═O bond rehybridization, O−H bond formation, and C−H bond dissociation all occur in concert along the approach to the transition state energy, and that H atom transfer is nearly complete by the time the barrier energy is reached. A final difference between the transition states determined using the RPBE+U and M06-L functionals is visible in the orientation of the reacting propene molecule. M06-L predicts stronger attractive interactions between the propene reactant and the catalyst, particularly with the bismuth atom adjacent to the active site. Thus, in the M06-L reaction path, the propene molecule sits more squarely over the adjacent bismuth atom. The RPBE+U calculation captures essentially no dispersive interactions and thus orients the propene into a sterically uncrowded site with no specific surface−adsorbate interactions.

Although it is not possible at present to investigate the geometric structure of a transition state in a heterogeneous catalyst experimentally, there exists sufficient experimental evidence to determine which transition state structure is more likely to represent the real chemistry in this particular system. In the RPBE+U calculation, the entirety of the activation energy supplied goes into rehybridization of an Mo═O bond; once this is accomplished, the hydrogen abstraction step is energetically downhill. If this were true in reality, then the homolytic bond dissociation energy of the C−H bond in

dx.doi.org/10.1021/jp409479h | J. Phys. Chem. C 2013, 117, 25562−25578

propene would play no role in determining the activation barrier. In that case, any hydrocarbon with a homolytic C−H bond dissociation energy less than or equal to that of propene would react over this catalyst with the same intrinsic activation energy. This prediction is contradicted by experimental evidence demonstrating that the apparent activation energies for oxidation of propene, 1-butene, 2-butene, and isobutene over bismuth molybdate differ significantly from each other.[132] Furthermore, the apparent activation energies for these olefins have been shown to correlate with their homolytic C−H bond dissociation energies.[133] The existence of such a correlation suggests that C−H bond dissociation must begin during the approach to the transition state, in line with the prediction from the M06-L functional. Thus, the transition state structure predicted by the M06-L functional provides better agreement with experimental trends than the transition state structure predicted by the RPBE+U functional.

The M06-L functional predicts an intrinsic reaction barrier of 32.3 kcal/mol, which when combined with a calculated heat of adsorption of 4.4 kcal/mol would lead to an apparent barrier of ∼27.9 kcal/mol. This result is higher than the experimentally reported values of 17−21 kcal/mol, though about half the difference results from the underestimated heat of propene adsorption. In considering just the intrinsic activation energy, a U_{eff} value near 7.5 eV would be required to yield an intrinsic barrier as low as 32.3 kcal/mol via RPBE+U calculations. Compared to the results obtained using the uncorrected RPBE, calculations performed using the M06-L functional give a barrier far closer to the experimental result (see Table 7).

Also notable is the energy of the final state in the M06-L calculation. The effect of the $+U_{eff}$ correction on the final state energy in RPBE+U calculations is similar to (actually slightly greater than) the effect on the barrier height; as a result, the energy of the final state is 17−24 kcal/mol lower than the highest energy along the reaction path for all values of U_{eff}. By contrast, the final state energy in the M06-L calculation is approximately 7 kcal/mol lower than the barrier energy. Given that the final state produced by hydrogen abstraction involves a free allyl radical, it is reasonable that this final state should be relatively high in energy. Thus, while the energies predicted by M06-L are higher than those obtained from experiment, the relative energy of the transition state versus the final state is chemically sensible.

5.0. CONCLUSIONS

This work has shown that the structure and electronic properties of RTMOs determined by DFT are very sensitive to the functional used for the calculations. A large part of this error arises from the self-interaction error and failure to capture properly the effects of van der Waals interactions between the adsorbate and the adsorbent. The results of the present investigation show that the performance of the M06-L functional matches or exceeds that of RPBE(+U) for every "ideal density functional" criterion except computational cost for which it exceeds RPBE+U by a factor of 4−5. These results are particularly impressive in the context of the systems investigated here: reducible transition metal oxides containing unpaired d electrons, which are particularly challenging to model using DFT due to the potentially large electron self-interaction errors such systems produce.

For calculations on MoO_2, adding a U_{eff} correction to RPBE calculations worsens the agreement between the calculated and experimentally measured electronic structures and also slightly worsens the predicted lattice constants. The M06-L functional provides superior results for lattice constants versus RPBE(+U) and an electronic structure in agreement with experimental data. For MoO_3, a U_{eff} correction has little effect on the geometry or electronic structure; however, the inability of RPBE(+U) to capture dispersive interactions leads to very significant errors in the lattice constants for all values of U_{eff}. The M06-L functional provides far better agreement with experimentally measured lattice constants, while providing an underestimate of the band gap similar to that seen in RPBE. For $Bi_2Mo_3O_{12}$, M06-L again provides more accurate lattice constants than RPBE(+U). For $Bi_2Mo_3O_{12}$, the band gap, the electronic structure of the hydrogen-reduced surface, and the calculated barriers for propene activation are all strong functions of the value of U_{eff}. However, no single value of U_{eff} provides accurate results for all of these properties. A U_{eff} value of 7.5 eV is required to match the experimentally observed band gap, and a U_{eff} value of 8.6 eV is required to provide good agreement with experiment for the observed activation barrier in propene oxidation over this material. At the same time, the transition-state structure produced when U_{eff} = 8.6 eV suggests that olefin activation should be independent of the C−H bond strength of the activated bond, which is in contradiction of experimental results. Furthermore, U_{eff} values above 4.0 eV provide increasingly poor descriptions of the electronic structure of the partially reduced catalyst. RPBE(+U) also dramatically underestimates the heat of adsorption of propene on the (010) surface of $Bi_2Mo_3O_{12}$. The M06-L functional also underestimates the band gap and the heat of adsorption of propene but in both cases produces far better values than RPBE functional. The activation barrier for propene oxidation is overestimated compared to experiment; however, the geometric structure of the transition state predicted by M06-L is in better agreement with experimentally observed olefin oxidation trends. The electronic structure of the partially reduced catalyst surface is also consistent with expectations based on available experimental data.

In conclusion, for moderately greater computational expense than that required for DFT+U, the M06-L functional provides reasonable geometries, electronic structures, and energies of reaction without requiring a user-provided tuning parameter. Significantly, for studies of chemical reactions occurring on surfaces of RTMOs, the M06-L functional provides not only reasonable reaction barriers but also reasonable heats of adsorption. Its ability to capture dispersive interactions may also recommend it for applications in which hydrogen bonding plays an important role, for example, for aqueous electrochemical systems. Although further testing for other RTMOs is required, this work shows that M06-L is capable of providing reliable, chemically insightful results on at least one family of RTMOs. Given the importance of these materials in catalysis and the challenges in describing them encountered using conventional DFT, the prospect of an improved method for obtaining accurate computational results in such systems provides significant incentive for further investigation.

■ ASSOCIATED CONTENT

Supporting Information

A plot of the electronic density of states in $Bi_2Mo_3O_{12}$ calculated using the M06-L and RPBE(+U) density functionals. This material is available free of charge via the Internet at http://pubs.acs.org.

AUTHOR INFORMATION

Corresponding Author

*E-mail: bell@uclink.berkeley.edu.

Notes

The authors declare no competing financial interest.

ACKNOWLEDGMENTS

Calculations performed in this work were conducted at the National Energy Research Scientific Computing Center (NERSC), which is supported by the Office of Basic Science of the U.S. Department of Energy under Contract No. DE-AC02-05CH11231. Additional calculations were performed at the University of California Berkeley Molecular Graphics and Computation Facility, which is supported by NSF Grant CHE-0840505. Funding for this work is provided by the Office of Basic Science of the U.S. Department of Energy under Contract No. DE-AC03-76SF00098. The authors would also like to thank Joseph Gomes and Professor Martin Head-Gordon of the University of California Berkeley for useful discussions.

REFERENCES

(1) Albonetti, S.; Cavani, F.; Trifirò, F. Key Aspects of Catalyst Design for the Selective Oxidation of Paraffins. *Catal. Rev.: Sci. Eng.* **1996**, *38* (4), 413−438.

(2) Vining, W. C.; Goodrow, A.; Strunk, J.; Bell, A. T. An experimental and theoretical investigation of the structure and reactivity of bilayered $VO_x/TiO_x/SiO_2$ catalysts for methanol oxidation. *J. Catal.* **2010**, *270* (1), 163−171.

(3) Zhang, W.; Desikan, A.; Oyama, S. T. Effect of Support in Ethanol Oxidation on Molybdenum Oxide. *J. Phys. Chem.* **1995**, *99*, 11468−11476.

(4) Chen, L.; Li, J.; Ge, M.; Zhu, R. Enhanced activity of tungsten modified CeO_2/TiO_2 for selective catalytic reduction of NO_x with ammonia. *Catal. Today* **2010**, *153* (3−4), 77−83.

(5) Lietti, L.; Forzatti, P.; Bregani, F. Steady-State and Transient Reactivity Study of TiO_2-Supported V_2O_5-WO_3 De-NO_x Catalysts: Relevance of the Vanadium-Tungsten Interaction on the Catalytic Activity. *Ind. Eng. Chem. Res.* **1996**, *35*, 3884−3892.

(6) Dunn, J. P.; Stenger, H. G., Jr.; Wachs, I. E. Oxidation of sulfur dioxide over supported vanadia catalysts: molecular structure − reactivity relationships and reaction kinetics. *J. Catal.* **1999**, *181* (2), 233−243.

(7) Kudo, A.; Miseki, Y. Heterogeneous photocatalyst materials for water splitting. *Chem. Soc. Rev.* **2009**, *38*, 253−278.

(8) Batzill, M. Fundamental aspects of surface engineering of transition metal oxide photocatalysts. *Energy Environ. Sci.* **2011**, *4*, 3275−3286.

(9) Amakawa, K.; Wrabetz, S.; Kröhnert, J.; Tzolova-Müller, G.; Schlögl, R.; Trunschke, A. In Situ Generation of Active Sites in Olefin Metathesis. *J. Am. Chem. Soc.* **2012**, *134* (28), 11462−11473.

(10) Bouchmella, K.; Mutin, P. H.; Stoyanova, M.; Poleunis, C.; Eloy, P.; Rodemerck, U.; Gaigneaux, E. M.; Debecker, D. P. Olefin metathesis with mesoporous rhenium-silicium-aluminum mixed oxides obtained via a one-step non-hydrolytic sol-gel route. *J. Catal.* **2013**, *301*, 233−241.

(11) Widmann, D.; Liu, Y.; Schüth, F.; Behm, R. J. Support effects in the Au-catalyzed CO oxidation − Correlation between activity, oxygen storage capacity, and support reducibility. *J. Catal.* **2010**, *276*, 292−305.

(12) Kim, H. Y.; Lee, H. M.; Henkelman, G. CO Oxidation Mechanism on CeO_2-Supported Au Nanoparticles. *J. Am. Chem. Soc.* **2012**, *134* (3), 1560−1570.

(13) Park, J. B.; Graciani, J.; Evans, J.; Stacchiola, D.; Ma, S.; Liu, P.; Nambu, A.; Fernández, S.; Hrbek, J.; Rodriguez, J. A. High catalytic activity of $Au/CeO_x/TiO_2$ (110) controlled by the nature of the mixed metal oxide at the nanometer level. *Proc. Natl. Acad. Sci. U.S.A.* **2009**, *106* (13), 4975−4980.

(14) Sanchez, A.; Abbet, S.; Heiz, U.; Scheider, W.-D.; Häkkinen, H.; Barnett, R. N.; Landman, U. When Gold Is Not Noble: Nanoscale Gold Catalysis. *J. Phys. Chem. A* **1999**, *103* (48), 9573−9578.

(15) Kimble, M. L.; Castleman, A. W., Jr.; Mitrić, R.; Bürgel, C.; Bonaĉić-Koutecký, V. Reactivity of Atomic Gold Anions toward Oxygen and the Oxidation of CO: Experiment and Theory. *J. Am. Chem. Soc.* **2004**, *126* (8), 2526−2535.

(16) van Santen, R.; Neurock, M. Concepts in theoretical heterogeneous catalytic reactivity. *Catal. Rev.: Sci. Eng.* **1995**, *37* (4), 557−698.

(17) Greeley, J.; Nørskov, J. K.; Mavrikakis, M. Electronic structure and catalysis on metal surfaces. *Annu. Rev. Phys. Chem.* **2002**, *53*, 319−348.

(18) Bell, A. T.; Head-Gordon, M. Quantum Mechanical Modeling of Catalytic Processes. *Annu. Rev. Chem. Biomol. Eng.* **2011**, *2*, 453−477.

(19) Zimmerman, P. M.; Tranca, D. C.; Gomes, J.; Lambrecht, D. S.; Head-Gordon, M.; Bell, A. T. Ab Initio Simulations Reveal that Reaction Dynamics Strongly Affect Product Selectivity for the Cracking of Alkanes over H-MFI. *J. Am. Chem. Soc.* **2012**, *134* (47), 19468−19476.

(20) Cohen, A. J.; Mori-Sánchez, P.; Yang, W. Insights into current limitations of density functional theory. *Science* **2008**, *321*, 792−794.

(21) Reuter, K.; Frenkel, D.; Scheffler, M. The steady state of heterogeneous catalysis, studied by first-principles statistical mechanics. *Phys. Rev. Lett.* **2004**, *93* (11), 116105.

(22) Teschner, D.; Novell-Leruth, G.; Farra, R.; Knop-Gericke, A.; Schlögl, R.; Szentmiklósi, L.; Hevia, M. G.; Soerijanto, H.; Schomäcker, R.; Pérez-Ramírez, J.; López, N. In situ coverage analysis of RuO_2-catalyzed HCl oxidation reveals the entropic origin of compensation in heterogeneous catalysis. *Nature Chem.* **2012**, *4* (9), 739−745.

(23) Hofmann, J. P.; Zweidinger, S.; Seitsonen, A. P.; Farkas, A.; Knapp, M.; Balmes, O.; Lundgren, E.; Andersen, J. N.; Over, H. Dynamic response of chlorine atoms on a RuO_2(110) model catalyst surface. *Phys. Chem. Chem. Phys.* **2010**, *12*, 15358−15366.

(24) Chrétien, S.; Metiu, H. Density functional study of the CO oxidation on a doped rutile TiO_2(110): Effect of ionic Au in catalysis. *Catal. Lett.* **2006**, *107* (3−4), 143−147.

(25) Pacchioni, G. Modeling doped and defective oxides in catalysis with density functional theory methods: Room for improvements. *J. Chem. Phys.* **2008**, *128*, 182505.

(26) Ganduglia-Pirovano, M. V.; Hofmann, A.; Sauer, J. Oxygen vacancies in transition metal and rare earth oxides: Current state of understanding and remaining challenges. *Surf. Sci. Rep.* **2007**, *62* (6), 219−270.

(27) Dudarev, S. L.; Botton, G. A.; Savrasov, S. Y.; Humphreys, C. J.; Sutton, A. P. Electron-energy-loss spectra and the structural stability of nickel oxide: An LSDA+U study. *Phys. Rev. B* **1998**, *57* (3), 1505−1509.

(28) Terakura, K.l; Oguchi, T.; Williams, A. R.; Kübler, J. Transition-metal monoxides: Band or Mott insulators. *Phys. Rev. Lett.* **1984**, *52*, 1830.

(29) Mori-Sánchez, P.; Cohen, A. J.; Yang, W. Localization and delocalization errors in density functional theory and implications for band-gap prediction. *Phys. Rev. Lett.* **2008**, *100*, 146401.

(30) Zhang, Y.; Yang, W. A challenge for density functionals: Self-interaction error increases for systems with a noninteger number of electrons. *J. Chem. Phys.* **1998**, *109*, 2604−2608.

(31) Feibelman, P. J.; Hammer, B.; Nørskov, J. K.; Wagner, F.; Scheffler, M.; Stumpf, R.; Watwe, R.; Dumesic, J. The CO/Pt(111) puzzle. *J. Phys. Chem. B* **2001**, *105*, 4018−4025.

(32) Kresse, G.; Gil, A.; Sautet, P. Significance of single-electron energies for the description of CO on Pt(111). *Phys. Rev. B* **2003**, *68*, 073401.

(33) Rossmeisl, J.; Qu, Z.-W.; Kroes, G.-J.; Nørskov, J. K. Electrolysis of water on oxide surfaces. *J. Electroanal. Chem.* **2007**, *607* (1−2), 83−89.
(34) Mosey, N. J.; Carter, E. A. Ab initio evaluation of Coulomb and exchange parameters for DFT+U calculations. *Phys. Rev. B* **2007**, *76*, 155123.
(35) Mosey, N. J.; Liao, P.; Carter, E. A. Rotationally invariant ab initio evaluation of Coulomb and exchange parameters for DFT+U calculations. *J. Chem. Phys.* **2008**, *129*, 014103.
(36) Cococcioni, M.; de Gironcoli, S. Linear response approach to the calculation of the effective interaction parameters in the LDA+U method. *Phys. Rev. B* **2005**, *71*, 035105.
(37) Kulik, H. J.; Cococcioni, M.; Scherlis, D. A.; Marzari, N. Density functional theory in transition-metal chemistry: a self-consistent Hubbard U approach. *Phys. Rev. Lett.* **2006**, *97*, 103001.
(38) Wang, L.; Maxisch, T.; Ceder, G. Oxidation energies of transition metal oxides within the GGA+U framework. *Phys. Rev. B* **2006**, *73*, 195107.
(39) Lutfalla, S.; Shapovalov, V.; Bell, A. T. Calibration of the DFT/GGA+U Method for Determination of Reduction Energies for Transition Metal and Rare Earth Metal Oxides of Ti, V, Mo, and Ce. *J. Chem. Theory Comput.* **2011**, *7*, 2218−2223.
(40) Scanlon, D. O.; Walsh, A.; Morgan, B. J.; Watson, G. W. An ab initio Study of Reduction of V_2O_5 through the Formation of Oxygen Vacancies and Li Intercalation. *J. Phys. Chem. C* **2008**, *112* (26), 9903−9911.
(41) Aschauer, U.; He, Y.; Cheng, H.; Li, S.-C.; Diebold, U.; Selloni, A. Influence of Subsurface Defects on the Surface Reactivity of TiO_2: Water on Anatase (101). *J. Phys. Chem C* **2010**, *114*, 1278−1284.
(42) Coquet, R.; Willock, D. J. The (010) surface of α-MoO_3, a DFT +U study. *Phys. Chem. Chem. Phys.* **2005**, *7*, 3819−3828.
(43) Loschen, C.; Carrasco, J.; Neyman, K. M.; Illas, F. First-principles LDA+U and GGA+U study of cerium oxides: Dependence on the effective U parameter. *Phys. Rev. B* **2007**, *75*, 035115.
(44) Nolan, M.; Fearon, J. E.; Watson, G. W. Oxygen vacancy formation and migration in ceria. *Solid State Ionics* **2006**, *177* (35−36), 3069−3074.
(45) Getsoian, A.; Shapovalov, V.; Bell, A. T. DFT+U Investigation of Propene Oxidation over Bismuth Molybdate: Active Sites, Reaction Intermediates, and the Role of Bismuth. *J. Phys. Chem. C* **2013**, *117* (14), 7123−7137.
(46) Shapovalov, V.; Fievez, T.; Bell, A. T. A Theoretical Study of Methanol Oxidation Catalyzed by Isolated Vanadia Clusters Supported on the (101) Surface of Anatase. *J. Phys. Chem. C* **2012**, *116*, 18728−18735.
(47) Zhang, Z.; Tang, W.; Neurock, M.; Yates, J. T., Jr. Electric Charge of Single Au Atoms Adsorbed on TiO_2(110) And Associated Band Bending. *J.. Phys. Chem. C* **2011**, *115* (48), 23848−23853.
(48) Scherlis, D. A.; Cococcioni, M.; Sit, P.; Marzari, N. Simulation of Heme Using DFT+U: A Step toward Accurate Spin-State Energetics. *J. Phys. Chem. B* **2007**, *111* (25), 7384−7391.
(49) Becke, A. D. Density-functional thermochemistry. III. The role of exact exchange. *J. Chem. Phys.* **1993**, *98*, 5648.
(50) Muscat, J.; Wander, A.; Harrison, N. M. On the prediction of band gaps from hybrid functional theory. *Chem. Phys. Lett.* **2001**, *342*, 397−401.
(51) Heyd, J.; Peralta, J. E.; Scuseria, G. E.; Martin, R. L. Energy band gaps and lattice parameters evaluated with the Heyd-Scuseria-Ernzerhof hybrid functional. *J. Chem. Phys.* **2005**, *123*, 174101.
(52) Andriotis, A. N.; Mpourmpakis, G.; Lisenkov, S.; Scheez, R. M.; Menon, M. U-calculation of the LSDA+U functional using the hybrid B3LYP and HSE functionals. *Phys. Status Solidi B* **2013**, *250* (2), 356−363.
(53) Moussa, J. E.; Schultz, P. A.; Chelikowsky, J. R. Analysis of the Heyd-Scuseria-Ernzerhof density functional parameter space. *J. Chem. Phys.* **2012**, *136*, 204117.
(54) Paier, J.; Marsman, M.; Kresse, G. Why does the B3LYP hybrid functional fail for metals? *J. Chem. Phys.* **2007**, *127*, 024103.
(55) Haunschild, R.; Odashima, M. M.; Scuseria, G. E.; Perdew, J. P.; Capelle, K. Hyper-generalized-gradient functionals constructed from the Lieb-Oxford bound: Implementation via local hybrids and thermochemical assessment. *J. Chem. Phys.* **2012**, *136*, 184102.
(56) Chai, J.-D.; Head-Gordon, M. Long-range corrected double-hybrid density functionals. *J. Chem. Phys.* **2009**, *131*, 174105.
(57) Peverati, R.; Truhlar, D. G. Improving the Accuracy of Hybrid Meta-GGA Density Functionals by Range Separation. *J. Phys. Chem. Lett.* **2011**, *2* (21), 2810−2817.
(58) Zhao, Y.; Truhlar, D. G. A new local density functional for main-group thermochemistry, transition metal bonding, thermochemical kinetics, and noncovalent interactions. *J. Chem. Phys.* **2006**, *125*, 194101.
(59) Zhao, Y.; Truhlar, D. G. The M06 suite of density functionals for main group thermochemistry, thermochemical kinetics, noncovalent interactions, excited states, and transition elements: two new functionals and systematic testing of four M06-class functionals and 12 other functionals. *Theor. Chem. Acc.* **2008**, *120*, 215−241.
(60) Goerigk, L.; Grimme, S. A thorough benchmark of density functional methods for general main group thermochemistry, kinetics, and noncovalent interactions. *Phys. Chem. Chem. Phys.* **2011**, *13*, 6670−6688.
(61) Hao, P.; Sun, J.; Xiao, B.; Ruzsinsky, A.; Csonka, G. I.; Tao, J.; Glindmeyer, S.; Perdew, J. P. Perforance of meta-GGA Functionals on General Main Group Thermochemistry, Kinetics, and Noncovalent Interactions. *J. Chem. Theory Comput.* **2013**, *9* (1), 355−363.
(62) Śliwa, P.; Handzlik, J. Assessment of density functionals for the study of olefin metathesis catalyzed by ruthenium alkylidene complexes. *Chem. Phys. Lett.* **2010**, *493* (4−6), 273−278.
(63) Ansbacher, T.; Srivastava, H. K.; Martin, J. M. L.; Shurki, A. Can DFT methods correctly and efficiently predict the coordination number of copper(I) complexes? A case study. *J. Comput. Chem.* **2009**, *31* (1), 75−83.
(64) Diesendrick, C. E.; Tzur, E.; Ben-Asuly, A.; Goldberg, I.; Straub, B. F.; Lemcoff, N. G. Predicting the Cis-Trans Dichloro Configuration of Group 15-16 Chelated Ruthenium Olefin Metathesis Complexes: A DFT and Experimental Study. *Inorg. Chem.* **2009**, *48* (22), 10819−10825.
(65) Jacobsen, H.; Cavallo, L. On the Accuracy of DFT Methods in Reproducing Ligand Substitution Energies for Transition Metal Complexes in Solution: The Role of Dispersive Interactions. *Chem. Phys. Chem.* **2012**, *13* (2), 562−569.
(66) Wannakao, S.; Boekfa, B.; Khongpracha, P.; Probst, M.; Limtrakul, J. Oxidative Dehydrogenation of Propane over a VO_2-Exchanged Zeolite: A DFT Study. *Chem. Phys. Chem.* **2010**, *11* (16), 3432−3438.
(67) Zhao, Y.; Truhlar, D. G. Benchmark Energetic Data in a Model System for Grubbs II Metathesis Catalysis and Their Use for the Development, Assessment, and Validation of Electronic Structure Methods. *J. Chem. Phys.* **2009**, *130*, 074103.
(68) Luo, S.; Zhao, Y.; Truhlar, D. G. Improved CO Adsorption Energies, Site Preferences, and Surface Formation Energies from a Meta-Generalized Gradient Approximation Exchange-Correlation Functional, M06-L. *J. Phys. Chem. Lett.* **2012**, *3* (20), 2975−2979.
(69) Mortensen, J. J.; Hansen, L. B.; Jacobsen, K. W. Real-space grid implementation of the projector augmented wave method. *Phys. Rev. B.* **2005**, *71*, 035109.
(70) Enkovaara, J.; et al. Electronic structure calculations with GPAW: a real-space implementation of the projector augmented-wave method. *J. Phys.: Condens. Matter* **2010**, *22*, 253202.
(71) Vilhelmsen, L. B.; Hammer, B. Systematic Study of Au_6 to Au_{12} Gold Clusters on MgO(100) *F* Centers Using Density-Functional Theory. *Phys. Rev. Lett.* **2012**, *108*, 126101.
(72) Ferrighi, L.; Madsen, G. K. H.; Hammer, B. Self-consistent meta-generalized gradient approximation study of adsorption of aromatic molecules on noble metal surfaces. *J. Chem. Phys.* **2011**, *135*, 084704.

(73) Katrib, A.; Leflaive, P.; Hilaire, L.; Maire, G. Molybdenum based catalysts. I. MoO_2 as the active species in the reforming of hydrocarbons. *Catal. Lett.* **1996**, *38*, 95−99.
(74) Wen, W.; Jing, L.; White, M. G.; Marinkovic, N.; Hanson, J. C.; Rodriguez, J. A. In situ time-resolved characterization of novel Cu-MoO_2 catalysts during the water-gas shift reaction. *Catal. Lett.* **2007**, *113* (1−2), 1−6.
(75) Grabowski, R.; Grzybowska, B.; Samson, K.; Sloczynski, J.; Stoch, J.; Wcislo, K. Effect of alkaline promoters on the catalytic activity of V_2O_5/TiO_2 and MoO_3/TiO_2 catalysts in oxidative dehydrogenation of propane and in isopropanol descomposition. *App. Cat. A* **1995**, *125* (1), 129−144.
(76) Chen, K.; Xie, S.; Iglesia, E.; Bell, A. T. Structure and Properties of Oxidative Dehydrogenation Catalysts Based on MoO_3/Al_2O_3. *J. Catal.* **2000**, *189* (2), 421−430.
(77) Smith, M. R.; Ozkan, U. S. The Partial Oxidation of Methane to Formaldehyde: Role of Different Crystal Planes of MoO_3. *J. Catal.* **1993**, *141*, 124−139.
(78) Grasselli, R. K. Advances and future trends in selective oxidation and ammoxidation catalysis. *Catal. Today* **1999**, *49*, 141−153.
(79) Nolan, M.; Watson, G. W. The electronic structure of alkali doped alkaline earthe metal oxides: Li doping of MgO studied with DFT-GGA and GGA+U. *Surf. Sci.* **2005**, *586* (1−3), 25−37.
(80) Yeriskin, I.; Nolan, M. Doping of ceria surfaces with lanthanum: a DFT+U study. *J. Phys.: Condens. Matt.* **2010**, *22* (13), 135004.
(81) Lei, Y.-H.; Chen, Z.-X. DFT+U study of properties of MoO_3 and hydrogen adsorption on MoO_3(010). *J. Phys. Chem. C* **2012**, *116*, 25757−25764.
(82) Perdew, J. P.; Schmidt, K. In *Density Functional Theory and Its Applications to Materials*; Van Doren, V. E.; Van Alsenoy, K.; Geerlings, P.; Eds.; American Institute of Physics: Melville, NY, 2001; p 1.
(83) Schmider, H. L.; Becke, A. D. Chemical content of the kinetic energy density. *J. Mol. Struct.* **2000**, *527*, 51−61.
(84) Becke, A. D. Simulation of delocalized exchange by local density functionals. *J. Chem. Phys.* **2000**, *112* (9), 4020−4026.
(85) Becke, A. D. A new inhomogeneity parameter in density-functional theory. *J. Chem. Phys.* **1998**, *109* (6), 2092−2098.
(86) Paier, J.; Marsman, M.; Hummer, K.; Kresse, G.; Gerber, I. C.; Ángyán, J. G. Screened hybrid density functionals applied to solids. *J. Chem. Phys.* **2006**, *125*, 249901.
(87) Heyd, J.; Scuseria, G. E.; Ernzerhof, M. Hybrid functionals based on a screened Coulomb potential. *J. Chem. Phys.* **2003**, *118*, 8207.
(88) There are actually several variants of the Heyd-Scuseria-Ernzerhof functional. The functional as originally proposed is now called HSE03 (ref 87). A follow-up paper in 2006 (ref 86) corrects a minor error in the construction of the original functional and uses a more optimal range separation parameter. The resulting functional is now generically called "HSE", but can be referred to as HSE06 when it needs to be distinguished from HSE03. Recently, Moussa et al. have systematically examined the range screening parameter and degree of exchange mixing to develop an optimal HSE variant called HSE12 (ref 53). In the present study, we use HSE to refer to the HSE06 variant of this functional.
(89) Perdew, J. P.; Ernzerhof, M.; Burke, K. The adiabatic connection method: a non-empirical hybrid. *J. Chem. Phys.* **1996**, *105* (22), 9982−9985.
(90) Technically, hybrid functionals like B3LYP, PBE0, HSE, and so forth calculate exact exchange using self-consistently derived Kohn−Sham orbitals, rather than self-consistently derived Hartree−Fock orbitals. It is therefore not entirely correct to refer to the resulting quantity as "Hartree Fock exchange." The distinction is not germane to the present discussion, but for the sake of rigor we retain the term "Hartree Fock-like exchange."
(91) Adamo, C.; Barone, V. Toward reliable density functional methods without adjustable parameters: The PBE0 model. *J. Chem. Phys.* **1999**, *110* (13), 6158−6170.
(92) Vydrov, O. A.; Heyd, J.; Krukau, A. V.; Scuseria, G. E. Importance of short-range versus long-range Hartree-Fock exchange for the performance of hybrid density functionals. *J. Chem. Phys.* **2006**, *125*, 074106.
(93) Krukau, A. V.; Vydrov, O. A.; Izmaylov, A. F.; Scuseria, G. E. Influence of the exchange screening parameter on the performance of screened hybrid functionals. *J. Chem. Phys.* **2006**, *125*, 224106.
(94) Kresse, G.; Furthmüller, J. Efficiency of ab-initio total energy calculations for metals and semiconductors using a plane-wave basis set. *Comput. Mater. Sci.* **1996**, *6*, 15.
(95) Perdew, J. P.; Burke, K.; Ernzerhof, M. Generalized Gradient Approximation Made Simple. *Phys. Rev. Lett.* **1996**, *77* (18), 3865−3868.
(96) Hammer, B.; Hansen, L. B.; Nørskov, J. K. Improved adsorption energetics within density-functional theory using revised Perdew-Burke-Ernzerhof functionals. *Phys. Rev. B* **1999**, *59* (11), 7413−7421.
(97) Dudarev, S. L.; Botton, G. A.; Savrasov, S. Y.; Szotek, Z.; Temmerman, W. M.; Sutton, A. P. Electronic Structure and Elastic Properties of Strongly Correlated Metal Oxides from First Principles: LSDA+U, SIC-LSDA and EELS Study of UO_2 and NiO. *Phys. Status Solidi A* **1998**, *166*, 429.
(98) Kresse, G.; Furthmüller, J. Efficient iterative schemes for ab initio total-energy calculations using a plane-wave basis set. *Phys. Rev. B* **1996**, *54*, 11169.
(99) Blochl, P. E. Projector augmented-wave method. *Phys. Rev. B* **1994**, *50*, 17953.
(100) Kresse, G.; Joubert, D. From ultrasoft pseudopotentials to the projector augmented-wave method. *Phys. Rev. B* **1999**, *59*, 1758.
(101) Sun, J.; Marsman, M.; Csonka, G. I.; Pruzsinszky, A.; Hao, P.; Kim, Y.-S.; Kresse, G.; Perdew, J. P. Self-consistent meta-generalized gradient approximation within the projector-augmented-wave method. *Phys. Rev. B* **2011**, *84*, 035117.
(102) Methfessel, M.; Paxton, A. T. High-precision sampling for Brillouin-zone integration in metals. *Phys. Rev. B* **1989**, *40*, 3616−3621.
(103) Blöchl, P. E.; Jepsen, O.; Andersen, O. K. Improved tetrahedron method for Brillouin-zone integrations. *Phys. Rev. B* **1994**, *49*, 16223−16233.
(104) Eyert, V.; Horny, R.; Höck, K.-H.; Horn, S. Embedded Peierls instability and the electronic structure of MoO_2. *J. Phys.: Condens. Matter* **2000**, *12*, 4923−4946.
(105) *Landolt-Börstein − Group III Condensed Matter: Numerical Data and Fundamental Relationships in Science and Technology*; Springer: Berlin, 2000; Vol *41D*, pp 1−7.
(106) Harwig, H. A. On the Structure of Bismuthsesquioide: The α, β, γ, and δ-phase. *Z. Anorg. Allg. Chem.* **1978**, 151−166.
(107) Tyuterev, V. G.; Vast, N. Murnaghan's equation of state for the electronic ground state energy. *Comput. Mater. Sci.* **2006**, *38*, 350−353.
(108) Birch, F. Finite elastic strain of cubic crystals. *Phys. Rev.* **1947**, *71* (11), 809−824.
(109) Mills, G.; Jónsson, H. Quantum and thermal effects in H_2 dissociative adsorption: Evaluation of free energy barriers in multidimensional quantum systems. *Phys. Rev. Lett.* **1994**, *72*, 1124−1127.
(110) Bitzek, E.; Koskinen, P.; Gähler, F.; Moseler, M.; Gumbsch, P. Structural relaxation made simple. *Phys. Rev. Lett.* **2006**, *97*, 107201.
(111) Sheppard, D.; Terrell, R.; Henkelman, G. Optimization methods for finding minimum energy paths. *J. Chem. Phys.* **2008**, *128*, 134106.
(112) Wheeler, S. E.; Houk, K. N. Integration grid errors for meta-GGA-predicted reaction energies: Origin of grid errors for the M06 suite of functionals. *J. Chem. Theory Comput.* **2010**, *6*, 395−404.
(113) Martin Head-Gordon, personal communication.
(114) Henderson, T. M.; Izmaylov, A. F.; Scalmani, G.; Scuseria, G. E. Can short-range hybrids describe long-range-deendent properties? *J. Chem. Phys.* **2009**, *131*, 044108.
(115) Stroppa, A.; Kresse, G. The shortcomings of semi-local and hybrid functionals: what we can learn from surface science studies. *J. New. Phys.* **2008**, *10*, 063020.

(116) Biller, A.; Tamblyn, I.; Neaton, J. B.; Kronik, L. Electronic level alignment at a metal-molecule interface from a short-range hybrid functional. *J. Chem. Phys.* **2011**, *135*, 164706.
(117) Da Silva, J. L. F.; Ganduglia-Pirovano, M. V.; Sauer, J.; Bayer, V.; Kresse, G. Hybrid functionals applied to rare-earth oxides: The example of ceria. *Phys. Rev. B* **2007**, *75*, 045121.
(118) Yang, K.; Zheng, Z.; Zhao, Y.; Truhlar, D. G. Tests of the RPBE, revPBE, τ-HCTHhyb, ωB97X-D, and MOHLYP density functional approximations and 29 others against representative databases for diverse bond energies and barrier heights. *J. Chem. Phys.* **2010**, *132*, 164117.
(119) Goodenough, J. B. Metallic Oxides. In *Prog. Solid State Chem.*; Reiss, H., Ed.; Pergamon: Oxford, 1971; pp 145−399.
(120) Nisar, J.; Peng, X.; Ahuja, R. Origin of ferromagnetism in molybdenum dioxide from ab initio calculations. *Phys. Rev. B.* **2010**, *81*, 012402.
(121) Gulino, A.; Parker, S.; Jones, F. H.; Egdell, R. G. Influence of metal-metal bonds on electron spectra of MoO_2 and WO_2. *J. Chem. Soc., Faraday Trans.* **1996**, *92* (12), 2137−2141.
(122) Scanlon, D. O.; Watson, G. W.; Payne, D. J.; Atkinson, G. R.; Egdell, R. G.; Law, D. S. L. Theoretical and Experimental Study of the Electronic Structures of MoO_3 and MoO_2. *J. Phys. Chem. C* **2010**, *114* (10), 4636−4645.
(123) Nie, X.; Esopi, M. R.; Janik, M. J.; Asthagiri, A. Selectivity of CO_2 Reduction on Copper Electrodes: The Role of the Kinetics of Elementary Steps. *Angew. Chem., Int. Ed.* **2013**, *52* (9), 2459−2462.
(124) Madsen, G. K. H.; Ferrighi, L.; Hammer, B. Treatment of Layered Structures Using a Semilocal meta-GGA Density Functional. *J. Phys. Chem. Lett.* **2010**, *1*, 515−519.
(125) Snyder, T. P.; Hill, C. G., Jr. The mechanism for the partial oxidation of propylene over bismuth molybdate catalysts. *Catal. Rev.* **1989**, *31* (1−2), 43−95.
(126) Zhai Z.; Getsoian A.; Bell A. T. The kinetics of selective oxidation of propene on bismuth vanadium molybdenum oxide catalysts. *J. Catal.* **2013**, in press. http://dx.doi.org/10.1016/j.cat.2013.5.008.
(127) Stradella, L.; Vogliolo, G. Energetics of the Adsorption of Propene, Water, Dioxygen on Bismuth Molybdate (2:1). *Z. Phys. Chem.* **1983**, *137*, 99−110.
(128) Křivánek, M.; Jírů, P.; Strnad, J. Adsorption and heat of adsorption of propylene on a Bi-Mo oxide catalyst. *J. Catal.* **1971**, *23*, 259−269.
(129) Grzybowska, B.; Haber, J.; Marczewski, W.; Ungier, L. X-ray and ultraviolet-photoelectron spectra of bismuth molybdate catalysts. *J. Catal.* **1976**, *42*, 327−333.
(130) Irfan, I.; Ding, H.; Gao, Y.; Small, C.; Kim, D. Y.; Subbiah, J.; So, F. The effect of molybdenum trioxide inter-layer between indium tin oxide (ITO) and organic semiconductor on the energy level alignment. *Appl. Phys. Lett.* **2010**, *96*, 243307.
(131) Kanai, K.; Koizumi, K.; Ouchi, S.; Tsukamoto, Y.; Sakanoue, K.; Ouchi, Y.; Seki, K. Electronde structure of anode interface with molybdenum oxide buffer layer. *Org. Electron.* **2010**, *11*, 188−194.
(132) Adams, C. R.; Voge, H. H.; Morgan, C. Z.; Armstrong, W. E. Oxidation of butylenes and propylene over bismuth molybdate. *J. Catal.* **1964**, *3*, 379−386.
(133) Zhai Z.; Bell. A. T. To be submitted for publication.